Norwegian University of Life Sciences
Faculty of Environmental Sciences
and Natural Resource Management

Philosophiae Doctor (PhD)
Thesis 2018:55

An experimental study on rotor-wake interactions of wind turbines

Eksperimentelle undersøkelser av den turbulente vakestrømningen bak vindturbiner

Franz Volker Mühle

An experimental study on rotor-wake interactions of wind turbines

Eksperimentelle undersøkelser av den turbulente vakestrømningen bak vindturbiner

Philosophiae Doctor (PhD) Thesis

Franz Volker Mühle

Norwegian University of Life Sciences
Faculty of Environmental Sciences and Natural Resource Management

Ås 2018

Thesis number 2018:55
ISSN 1894-6402
ISBN 978-82-575-1762-5

PhD supervisors

Professor Muyiwa Samuel Adaramola
Faculty of Environmental Science and Natural Resource Management
Norwegian University of Life Sciences
Ås, Norway

Professor Lars Roar Sætran
Department of Energy and Process Engineering
Norwegian University of Life Sciences
Trondheim, Norway

Associate Professor Arne Reidar Gravdahl
Faculty of Environmental Science and Natural Resource Management
Norwegian University of Life Sciences
Ås, Norway

Evaluation committee

Professor Sandrine Aubrun-Sanches
Research Department
Centrale Nantes
Nantes, France

Professor Alberto Zasso
Department of Mechanical Engineering
Politecnico di Milano
Milan, Italy

Professor Erik Trømborg
Faculty of Environmental Science and Natural Resource Management
Norwegian University of Life Sciences
Ås, Norway

To my Mother

Acknowledgements

Many people have been involved in supervising and supporting this thesis, who I would like to express my gratitude to.

First of all I would like to thank my supervisors, Sam Adaramola Lars Sætran and Arne Gravdahl. Thank you, Sam for giving me the opportunity to work on this project and for providing me the freedom I needed to be creative. I always felt taken care of and knew your office door was open for any kind of discussion. Thank you, Lars for giving me the possibility to work at the place I enjoyed most during my PhD, the fluid mechanics laboratory at NTNU, and for welcoming me from the very beginning on as part of your team. It was always nice coming to your office and leaving with new ideas and questions to solve. Thank you, Arne for always showing interest in my work and your support when needed. I always knew that I had someone to support me if things would not work out.

I would like to thank the colleagues I collaborated with: Jan, Jannik and Thomas, without you the thesis would not have been possible in the way it is now. My special thanks go to Jan, there are so many things that come in my mind to thank you for that I cannot name all of them here. It was a great pleasure teaming up with you.

I would like to thank everyone at the Department of Energy and Process Engineering at NTNU for your hospitality. It was a great research stay with many enriching experiences.

I had a great time working at MINA and EPT, thanks to my office mates, my fellow PhD students and my colleagues. Thank you for brightening my life, also outside of work. Many thanks also tho the administrative staff at NMBU and NTNU for all their support.

A special thank goes to my family, for all the support you gave me in all kind of ways. It is important to know that there are people who will be always on you side, no matter what happens.

Finally, I would like to thank all my friends in Germany, Norway and all around the world. I am very lucky to have so many good friends. You all had your contribution to the thesis and it is most likely bigger as you would think. I would like to name all of

you here, but I am scared I would miss out half of the people after this whole thesis writing. But now that I am finished I will have more time and I am sure we will have the possibility to meet some time and I can thank you personally.

Ås, May 2018
Franz Mühle

Abstract

Interactions of wind turbine wakes with downstream turbines can reduce a wind farm's power production and increase loads on the individual turbines. For the purpose of wind farm optimization, different aerodynamic approaches to modify the performance and wake flow of one or two model wind turbines have been tested in a number of wind tunnel experiments.

In a first set of measurements, different modifications of the rotor design to limit wake effects are studied. Herein, the effect of the blade number on the wake development is studied by comparing the wake properties behind 2- and 3-bladed model wind turbines. Also, the influence of the rotational direction is investigated by comparing the performance of an aligned two-turbine array with co- and counter-rotating rotors. Moreover, the effect of winglets on the performance and vortex interaction in the wake is assessed. For this purpose, a new rotor with aerodynamically optimized winglets has been designed. The performance of the rotor is compared to a reference rotor without winglets and effects on the vortex interaction and velocity recovery in the wake are investigated.

The second set of measurements investigated the control of the model wind turbines by intentional yaw misalignment. Therefore, the wake flow behind a yawed turbine exposed to different inflow conditions is measured, while also the power and loads on a two-turbine array are analyzed for varying separation distances, lateral offsets and yaw angles. Selected test cases are furthermore provided for validation purposes of CFD codes. In a Blind test experiment, performance and wake data are compared to computational results from external groups.

All the experiments have been carried out in the closed-loop wind tunnel at NTNU in Trondheim. The wakes were investigated for uniformly distributed and sheared inflow velocity profiles with different turbulence intensities ranging from 0.23% to 10.0%. During the project different rotor designs from 2- to 3-bladed rotors, all with a diameter of $D = 0.9$ m, are investigated. The velocities in the wake are measured using a 2-component laser Doppler velocimetry system or a Cobra probe, which is used to extract phase-averaged information from the wake flow.

The potential of the blade number and opposite rotational directions in turbine array are found not to have a significant potential for the optimization of a wind farm. While not affecting the mean velocity distribution, the blade number is observed to influence to turbulence peak levels in the wake. An opposite rotation of the downstream turbine is assessed only to be effective for very small turbine separation distances, where the energy contained in the wake swirl of the upstream turbine can be extracted. The design of aerodynamically optimized winglets could rise the power coefficient C_P of a single rotor by 8.9%, whereas the thrust coefficient C_T only increased by 7.4%. Winglets are furthermore found to accelerate the tip vortex interaction in the wake, leading to a local shear layer enlargement and earlier wake recovery. In a wind farm, rotors with winglets extract more energy and leave a similar amount of kinetic energy in the wake for potential downstream turbines. Yaw control is found to have the largest potential for the optimization of wind farms. The total power of an aligned two-turbine array is assessed to increase up to 11% by deflecting the upstream turbine's wake laterally though an intentional yaw misalignment. However, yaw moments on yawed turbines and turbines operating in a partial wake are observed to increase, showing the importance of considering loads for yaw control. Finally, the comparison of experimental data to numerical predictions in the Blind test confirmed the strength of codes based on Large-Eddy Simulations (LES) in predicting mean velocity and turbulent kinetic energy levels in the wake precisely.

Table of contents

Abstract **vii**

List of figures **xi**

List of tables **xiii**

List of papers **xv**

Nomenclature **xix**

1 Introduction **1**

1.1 Motivation 1

1.1.1 Historic summary of wind turbine development 2

1.1.2 Wind turbine interactions 3

1.1.3 An introduction into the wind turbine wake 4

1.1.4 Wind farm optimization approaches 5

1.1.5 Wake investigation techniques 7

1.2 Objective 8

1.3 Thesis outline 10

2 Methodology **13**

2.1 Wind tunnel 13

2.1.1 Inflow conditions 14

2.1.2 Wind tunnel blockage 16

2.2 Model wind turbines 16

2.3 Model rotor design 18

2.3.1 Blade element momentum method 18

2.3.2 Rotors 23

2.3.3 3D printed blades for wind tunnel tests 27

2.3.4 Scaling effects 29

2.4 Measurement technique 30
2.4.1 Power measurement technique 30
2.4.2 Force measurement technique 32
2.4.3 Wake measurement technique 32
2.5 Measurement uncertainty 36

3 Summary of main results **39**
3.1 Wind farm optimization 39
3.1.1 Comparison of 2- and 3-bladed rotors 40
3.1.2 Counter rotating wind turbine rotors 42
3.1.3 Winglet rotor 43
3.1.4 Yaw wake control 46
3.2 Reference data for CFD validation 49
3.2.1 Blind test comparison 50

4 Conclusions **53**

References **57**

Appendix A Technical drawings **65**

Paper I **71**

Paper II **87**

Paper III **101**

Paper IV **127**

Paper V **155**

Paper VI **183**

Paper VII **211**

List of figures

1.1 Schematic wake flow, adapted from (Hau, 2013; S. Lissaman, 1979). . 5
1.2 The importance of wind tunnel experiments and the connection between the three wake measurement techniques. 9
1.3 Summary and connection of all papers in the thesis. 12

2.1 Test section of the wind tunnel with dimensions and coordinate system, looking in flow direction. 14
2.2 Different inlet configurations and resulting $U_\infty{}^*$ and TI in [%] at the turbine position for (a) low-turbulence uniform, (b) high-turbulence uniform and (c) high-turbulence shear inflow. 15
2.3 Model wind turbines (a) T2, (b) T1 and (c) LARS1, all equipped with the standard 3-bladed NTNU rotor. 17
2.4 Schematic stream tube describing the one-dimensional flow passing a wind turbine, with the corresponding pressure and velocity distribution. 20
2.5 Blade element with velocity triangle at the rotor plane and the resulting force R, with components for lift L and drag D and the load coefficients in axial and tangential direction. 21
2.6 Span-wise (a) chord length c and (b) twist angle θ distribution for the rotors used in the PhD study (r is the radial position). 23
2.7 Airfoil shapes used for the model rotors. 25
2.8 Predicted airfoil polars at $Re = 1.0{\cdot}10^5$ using XFOIL. 25
2.9 Model rotors for the experiment comparing the effect of the blade number on the wake development, mounted on model turbine T2 (taken from *Paper I*). 26
2.10 Model wind turbine rotor with exchangeable blade tips. 27
2.11 (a) C_P and (b) C_T for the 3-bladed rotor milled from Aluminum and 3D printed in VeroGray. 28

2.12 Deformation of the blade tip of the 3D printed 3-bladed rotor for $U_\infty = 10.0$ m/s at (a) $\lambda = 6$ and (b) $\lambda = 10$. With the blade deflection in x- and y-direction given in cm. 29
2.13 Picture of the turbine hub of T2 and a sketch of its cross-section showing the setting with the installed measurement technique (blue) inside the hub. 31
2.14 Calibration process of torque transducer. 31
2.15 Picture of the turbine hub and sketch of the setting with the installed measurement technique (blue) insight the hub. 33
2.16 Series 100 Cobra probe, with detailed probe head geometry and the flow axis system. 35
2.17 Simultaneous measurements with LDV and Cobra probe for adjustment of Cobra probe head. 36
2.18 Explanation of systematic and random error. 36

3.1 Contour plots of normalized streamwise mean velocity, with arrows representing the resultant of the vertical and horizontal velocity component, in the wake (a) $2.00D$, (b) $3.50D$ and (c) $5.15D$ behind the clock-wise rotating 3-bladed rotor mounted on turbine T2, the black lines represent the turbine rotor, nacelle and tower, locking in flow direction. 43
3.2 Winglet on the wing tip of a transport airplane. 44
3.3 Pressure equalization at the blade tip and the resulting tip vortex and lift distribution. 44
3.4 Sketch of forces induced by a yawed wind turbine and the resulting lateral wake deflection. 46

A.1 Technical drawing of NTNU model wind turbine T1. 66
A.2 Technical drawing of NTNU model wind turbine T2. 67
A.3 Technical drawing of NTNU model wind turbine LARS1. 68

List of tables

2.1 Key parameters of the rotors used in the PhD study, (tip speed ratio (λ) clock-wise (CW) and counter-clock-wise (CCW) rotation). 24
2.2 Relevant mechanical properties of blade materials Aluminum and VeroGray. 28

3.1 Summary of differences in available power (P_{ava}) and turbulence intensity (TI) in the wake behind the 3-bladed rotor (Rotor1), the 2-bladed rotor with the same aspect ratio (Rotor2) and the 2-bladed rotor with the same solidity (Rotor3). 41

List of papers

Paper I

The effect of the number of blades on wind turbine wake – a comparison between 2-and 3-bladed rotors

Mühle F, Adaramola MS and Sætran L

Published in Journal of Physics, Conference Series, vol. 753 (2016) 032017

doi: 10.1088/1742-6596/753/3/032017

The author's contribution: The rotors were designed and constructed by Mühle. The experimental work and the analysis of the data were performed by Mühle. The manuscript was written by Mühle and reviewed by Adaramola and Sætran. The project was supervised by Adaramola and Sætran. The paper was presented by Mühle at the Torque conference 2016 in Munich.

Paper II

The effect of rotational direction on the wake of a wind turbine rotor – an experimental comparison study of aligned co- and counter rotating turbine arrays

Mühle F, Adaramola MS and Sætran L

Published in Energy Procedia, vol. 137 (2017), pp. 238-245

doi: 10.1016/j.egypro.2017.10.346

The author's contribution: The experimental work and the analysis of the data were performed by Mühle. The manuscript was written by Mühle and reviewed by Adaramola and Sætran. The project was supervised by Adaramola and Sætran. The paper was presented by Mühle at the DeepWind conference 2017 in Trondheim.

Paper III

An experimental study on the effect of winglets on the tip vortex interaction in the near wake of a model wind turbine

Mühle F, Bartl J, Hansen T, Adaramola M S and Sætran L

Manuscript

The author's contribution: The rotor was designed by Mühle and Hansen and the winglet design was optimized by Hansen. The experiment was planned and performed by Mühle. The data was evaluated, analyzed and discussed by Mühle and Bartl. The manuscript was written by Mühle and Bartl and reviewed by Hansen. The project was supervised by Adaramola and Sætran.

Paper IV

Winglet Shape Optimisation for a Model-Scale Wind Turbine

Hansen T and Mühle F

Published in Wind Energy, vol. (2018), pp. 1-17

doi: 10.1002/we.2183

The author's contribution: The optimization and computational analysis was performed by Hansen. The rotor blade was designed by Hansen and Mühle. The construction of the wind tunnel models and the experimental testing was performed by Mühle. The evaluation and validation of the numerical results was performed by Hansen. The article was written by Hansen and reviewed by Mühle.

Paper V

Wind tunnel experiments on wind turbine wakes in yaw: Effects of inflow turbulence and shear

Bartl J, Mühle F, Schottler J, Sætran L, Peinke J, Adaramola M S and Hölling M

Accepted for publication in Wind Energy Science, 2018

doi: 10.5194/wes-2017-59

The author's contribution: The experiment was planned and performed by Bartl and Mühle. The data was evaluated, analyzed and discussed by Bartl, Mühle and Schottler. The manuscript was written by Bartl and reviewed by Mühle and Schottler. The project was supervised by Peinke, Hölling, Adaramola and Sætran.

Paper VI

Wind tunnel study on power and loads optimization of two yaw-controlled model wind turbines

Bartl J, Mühle F and Sætran L

In review in Wind Energy Science

doi: 10.5194/wes-2018-24

The author's contribution: The experiment was planned and performed by Bartl and Mühle. The data was evaluated, analyzed and discussed by Bartl and Mühle. The manuscript was written by Bartl and reviewed by Mühle. The project was supervised by Sætran.

Paper VII

Blind test 5 – the wake behind a yawed wind turbine

Mühle F, Schottler J, Bartl J, Futrzynski R, Evans S, Bernini L, Schito P, Draper M, Guggeri A, Kleusberg E, Henningson D, Hölling M, Peinke J, Adaramola M S and Sætran L

In review in Wind Energy Science

doi: 10.5194/wes-2018-30

The author's contribution: The experiments were planned and performed by Mühle, Bartl and Schottler. The data was evaluated, analyzed and discussed by Mühle, Bartl and Schottler. The numerical data was provided by co-authors Futrzynski, Evans, Bernini, Schito, Draper, Guggeri, Kleusberg and Henningson. The Blind test workshop was organized by Mühle and Bartl. The manuscript was written by Mühle and reviewed by Bartl and Schottler. The project was supervised by Peinke, Hölling, Adaramola and Sætran.

Additional papers

Paper VIII

Lidars for Wind Tunnels - an IRPWind Joint Experiment Project

Sjöholm M, Vignaroli A, Agelou N, Nielsen M B, Mann J, Mikkelsen T, Bolstad H C, Merz K O, Sætran L, Mühle F, Tiihonen M and Lehtomäki V

Published in Energy Procedia, vol. 137 (2017), pp. 339-345

doi: 10.1016/j.egypro.2017.10.358

Paper IX

Experiments in the wind turbine far wake for the evaluation of an analytical wake model

García L, Vatn M, Mühle F and Sætran L

Published in Journal of Physics, Conference Series, vol. 854 (2017) 012015

doi: 10.1088/1742-6596/854/1/012015

Paper X

Comparative study on the wake deflection behind yawed wind turbine models

Schottler J, Mühle F, Bartl J, Peinke J, Adaramola M S, Sætran L and Hölling M

Published in Journal of Physics, Conference Series, vol. 854 (2017) 012032
doi: 10.1088/1742-6596/854/1/012032

Paper XI

Wind tunnel experiments on wind turbine wakes in yaw: Redefining the wake width

Schottler J, Bartl J, Mühle F, Sætran L, Peinke J and Hölling M

Accepted for publication in Wind Energy Science, 2018
doi: 10.5194/wes-2017-58

Paper XII

A Detached-Eddy-Simulation study: Proper-Orthogonal-Decomposition of the wake flow behind a model wind turbine

Göing J, Bartl J, Mühle F, Sætran L, and Thamsen P U

Submitted to Journal of Physics, Conference Series, DeepWind 2018

Paper XIII

Experimental validation of analytical wake and downstream turbine performance modeling

Polster F, Bartl J, Mühle F, Thamsen P U and Sætran L

Submitted to Journal of Physics, Conference Series, DeepWind 2018

Paper XIV

Validation of the real-time-response ProCap measurement system for full field wake scans behind a yawed model-scale wind turbine

Bartl J, Müller A, Landolt A, Mühle F, Vatn M, Oggiano L and Sætran L

Submitted to Journal of Physics, Conference Series, DeepWind 2018

Nomenclature

Roman Symbols

A_{in}	Inlet area of the contraction nozzle
A_{out}	Outlet area of the contraction nozzle
A_R	Rotor swept area
a	Axial induction factor
a'	Tangential induction factor
B	Number of rotor blades
C_P	Power coefficient
C_T	Thrust coefficient
C_L	Lift coefficient
C_D	Drag coefficient
c	Chord length
D	Rotor diameter wind turbine
F	Prandtl's tip loss factor
f_D	Doppler frequency
M	Torque
n	Number of measurements
P	Power
p_{amb}	Ambient pressure

Δp	Pressure difference
R	Rotor radius wind turbine
Re	Reynolds number
B_R	Random uncertainty
r	Radial position
P_R	Systematic uncertainty
Δr	Radial blade element length
C_T	Thrust force
TI	Turbulence intensity
t	Student's t
$Temp$	Temperature
U_∞	Inlet velocity
U^*_∞	Normalized inlet velocity
$\bar{u}$	Time averaged velocity
u'	Turbulent velocity component
U_{ref}	Reference velocity
Δx	Fringe spacing interval
y_{ref}	Reference height

Greek Symbols

α	Power law coefficient
α_a	Angle of attack
β	Blade pitch angle
γ	Yaw angle
λ	Tip speed ratio
λ_{loc}	Local tip speed ratio

λ_{LDV}	Wave length laser beams LDV
ω	Rotational speed of the rotor
ω_R	Total uncertainty
φ	Flow angle
ρ	Air density
σ	Standard deviation
ν	Kinematic viscosity
σ_s	Solidity, fraction of blade covered area
θ	Blade twist angle

Superscripts

$*$	Normalized values

Acronyms / Abbreviations

BEM	Blade element momentum
CFD	Computational fluid dynamics
DAQ	Data acquisition
FFT	Fast Fourier Transformation
LiDAR	Light detection and ranging
LES	Large-eddy simulation
PIV	Particle image velocimetry
RANS	Reynolds-Averaged-Navier-Stokes
TKI	Turbulent kinetic energy

Chapter 1

Introduction

This section introduces the topic of wind energy and rotor wake interactions and explains the motivation for the PhD thesis. The important contribution of wind energy development to achieve the climate goals and to limit global warming is explained. Furthermore, the historic development of wind energy, which resulted in large turbines, which are clustered in wind farms onshore and offshore is summarized to show the success of previous research. Next, wind farm interactions, which affect the overall efficiency and increased turbine loading are explained to show the potential for wind farm optimization. Thereafter the turbine wake, which causes these interactions and is characterized by low velocities and increased turbulence is introduced. Then the measures, wind farm layout, rotor design and turbine control, which can be optimized to limit such wake effects are presented. The motivation is concluded with an introduction of the wake investigation techniques, wind tunnel tests, numerical simulations and measurements of full-scale wind turbines, which all have some limitations, but complement each other to provide accurate wake data. After the motivation, the objectives of the PhD thesis are explained. The main goal of the PhD thesis is to enhance the current knowledge of the physics of rotor wake interactions to improve wind farm efficiency. Finally, the thesis structure will be presented and the different papers are classified and connected.

1.1 Motivation

The consequences of the climate change are one of the major topics human kind is likely to face in future. Herein, the largest single source of global greenhouse gas emissions is the utilization of fossil fuels for the generation of electricity and heat (IPCC, 2014). Although the energy sector is already a major contributor to global warming, the world wide energy demand is expected to further increase in the next decades (IEA, 2017).

The political will to limit global warming has resulted in the Paris Agreement that was adopted in 2015. The agreement has the goal of saving the climate and limiting the increase in global average temperature below 2 °C compared to pre-industrial levels (UNFCCC, 2015). To achieve this two-degree goal the transition from fossil fuels to renewable energy sources is of major importance (IEA, 2016).

1.1.1 Historic summary of wind turbine development

Within the renewable energies, wind energy, with its vast potential plays a fundamental role in the energy transition. Wind energy has also a long history, which will be presented in the following overview that is adopted from Hau (2013) and Manwell et al. (2010). The first historical source goes back to the 7th century and tells of vertical axis wind mills that were used in Persia for milling grain. But also in China wind mills were already used for the irrigation of rice fields. The horizontal axis wind turbine, which is the common type today, is assumed to be invented in Europe in the 12th century. It was used all over Europe up into the 20th century mainly for milling, but with further development also for sawing wood and machining metal. The power generation with wind turbines began already in the end of the 19th century. The Danish professor Paul La Cour built a wind turbine driving a dynamo as early as 1891, this concept was further developed and utilized until the middle of the 20th century. Furthermore, La Cour is assumed to be the first researcher to carry out wind tunnel experiments on wind turbines in a self constructed facility. Until the 17th century, wind turbine development was no result of systematic research, but then physical and mathematical thinking became more established and scientists drafted the first works on wind mills. In the 1920's the aerodynamicist Albert Betz formulated the modern physical principles of wind energy conversion, he published his research in 1926 and provided basis for the aerodynamically design of wind turbine blades (Betz, 1926).

In the first part of the 20th century different turbine concepts were developed in Europe and the United States ranging from small turbines that where produced in a large quantity to experimental turbines with big rotors. The rotors had different number of blades ranging from 2-bladed to multiple bladed rotors and were manufactured from various materials like fabric, aluminum, stainless steel laminated wood and even glass-fiber composites. However, the low price of fossil fuels lead to decreasing interest in further development of windmills for energy generation. Consequently, most of the turbines where decommissioned in the 1960's as they where economically unprofitable.

However, the oil crisis in the 1970's changed the perspective on energy generation, as the price for fossil fuels increased and western countries wanted to become more independent from oil exports. Consequently, renewable energy sources became inter-

esting for electricity generation again. Therefore, the US government and European governments, especially Denmark, Sweden and Germany initialized various research programs to further develop wind power. In the 1980's, the focus was set primarily on large experimental turbines, which were mostly developed by well known industrial companies. The turbines were tested intensively the first years and were even kept running into the 1990's. Even though the large turbines were not very successful and thus the research focus on them came too early, they provided the technical foundation for modern wind turbine technology. Simultaneously, an interest in clustering wind turbines arose and as a result the first wind farms were built in California in the beginning of the 1980's. A large number of turbines in these wind farms were imported from Denmark, where companies started to build small 3-bladed turbines, after the energy crisis. These turbines were economically sustainable and were manufactured in a large number. Together with the first law supporting renewable energies in Germany, wind power became more and more important.

In the following decades, those turbines were further developed from a diameter of 15 m and a rated power of 50 kW to turbines with a diameter of up to 180 m and a rated power of up to 9.5 MW, which are actually used today (Windpowermonthly, 2017). Wind turbines are also not only installed on land but also more and more offshore. Between 2011 and 2017 the globally installed offshore capacity increased from around 4.000 MW to 18.000 MW (GWEC, 2017). The offshore wind marked is expected to further grow and with the successful development of floating wind turbines, high wind locations in deep water can be utilized for wind farm installations in the future. The successful history of wind energy for generating electricity and the importance of wind power can be seen in the globally installed wind power capacity, which is distributed to 90 countries and increased from 24.000 MW in 2001 to around 540.000 MW in 2017. Today, wind power is effectively competing with traditional energy sources and thus a further increase of installed capacity of over 800.000 MW globally is expected until 2021 (GWEC, 2017).

1.1.2 Wind turbine interactions

Most wind turbines today are installed in wind farms as the installation and maintenance costs are lower compared to a single turbine operation. However, the turbines cannot be arranged randomly and too close to each other. This is because the flow downstream of a wind turbine is characterized by a reduced mean flow velocity and an increased turbulence level. This flow field, behind the wind turbine, is called the wind turbine wake.

Experimental and numerical studies show that the velocity deficit in the wake is only minor after a separation distance of $10D$ (D is the rotor diameter) (Ammara et al., 2002). The higher turbulence however, is still present at a distance of $15D$ downstream of the rotor (Højstrup, 1999). In most wind farms, the typical spacing for turbines is between 4 - $8D$, as the installation costs would be too high for larger separation distances (Barthelmie et al., 2006). Consequently, the turbines are usually installed close enough that they interact with each other and the wake of the upstream turbine influences the downstream turbine's power production. Barthelmie et al. (2009) reported average losses of 10 - 20% between the first and second turbine row in a offshore installation and a maximum power drop of up to 35% in the extreme case when the turbines are aligned with the wind direction. In another study, Thomsen and Sørensen (1999) investigated fatigue loads in an offshore wind farm and found an increase of 5 - 15% for the whole wind farm compared to the free flow situation. Furthermore, Sanderse (2009) stated an increase of up to 80% in fatigue loading for turbines that were aligned with the wind direction. Because of this influence on wind farm performance and the large potential of wind farm optimization, the European Academy of Wind Energy (EAWE) listed wake investigations as one of the research challenges in their long-term wind energy research agenda (van Kuik et al., 2016).

1.1.3 An introduction into the wind turbine wake

The wake of a wind turbine is schematically depictured in Figure 1.1. It can be mainly divided into two different sections, the near wake and the far wake (S. Lissaman, 1979). The complex near wake region is characterized by pressure equalization of the low pressure, resulting from extracting energy by the rotor and the ambient air. As a result, the wake widens and the center line velocity decreases until it reaches its minimum (when the pressure in the wake is similar to the ambient pressure) at around 1 - $2D$ downstream (Ainslie, 1988). From there, fluid mixing dominates the wake flow, the high turbulence in the boundary layer that is caused by blade tip vortices, mixes with the higher velocity in the ambient flow, generating a shear layer that expands outwards and inwards until it reaches the center line at around 2 - $5D$. This point is defined as the end of the near wake (Crespo et al., 1999).

After the transition region where the wake velocity is further increasing and the tip vortices decay due to interaction with the ambient turbulence, the far wake begins at around $5D$. In the far wake the wake is fully developed and the velocity deficit in the center decays with a rate that is dependent on the ambient turbulence (Ainslie, 1988). In a hypothetical case with an uniform inflow, the velocity and turbulence profiles in the far wake are axissymmetric and distributed self similar (Crespo et al., 1999).

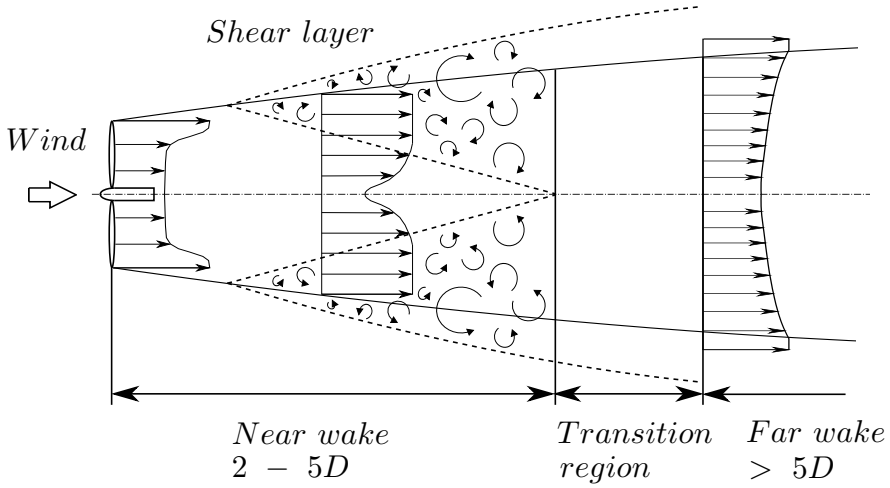

Figure 1.1: Schematic wake flow, adapted from (Hau, 2013; S. Lissaman, 1979).

1.1.4 Wind farm optimization approaches

Research on wind turbine wakes already started in the 1970's and since then several studies, investigating the wind turbine wake and its implication have been conducted. Detailed reviews about these studies and the wind turbine wake research can be found from Vermeer et al. (2003) and Sanderse (2009).

Understanding wakes and their structure in detail is important for the optimization of wind farms. Wake effects have to be considered when planning the arrangement of wind turbines and the operation of a wind farm can be optimized by taking turbine interactions into account. There are different approaches for optimizing the performance of a wind farm. These are mainly the wind farm layout, the turbine/rotor design and the wind farm control during operation. For the optimization of wind farms not every single turbine is optimized but the whole arrangement has to be as effective as possible. Thus, a single turbine might operate at a less efficient state and not extract the maximum energy from the wind, leaving more energy for downstream turbines, so that the whole farm can be more efficient.

The wind farm layout is offering a large potential for increasing overall performance. In a complex terrain it is determined mainly by the site's topography and the wind regime. Flat terrain and especially offshore sites offer better possibilities for a customized farm layout. Based on the layout, the wake impact on the downstream turbines could be improved using different approaches. Firstly, the separation distances among the turbines could be increased until the wake effects decayed before reaching the downstream turbine. The demand for land however would be very high and also installation and infrastructure would increase costs dramatically. Secondly, the turbine configuration can be varied by different approaches like an aligned array or structured

and unstructured grids. Consequently, many factors have to be taken into account finding the most efficient layout. Therefore, several studies optimizing the wind farm layout have been conducted. An initial optimization study on wind farm layout was conducted by Mosetti et al. (1994). The authors used the Jensen wake model to simulate a wind farm and optimized it for maximum energy and minimum installation cost. Since then, many studies using different approaches to optimize wind turbine arrays have been conducted. An overview of these approaches is given in the review by Shakoor et al. (2016).

The rotor design is another possibility to optimize a wind farm in the design process. Usually wind turbine rotors are designed to extract as much energy from the wind as possible. However, if they could be designed to leave more energy in the flow, the overall performance of a wind farm could benefit from that, because more energy would be available for downstream turbines operating in the wake. An example for such a rotor concept is the low-induction rotor, which is working at non optimal induction and thus has a lower efficiency. Such a rotor is mainly designed for load reduction but is also reducing wake effects (Quinn et al., 2016). Designing a rotor with the focus on limiting wake losses was not yet considered a lot within wind farm optimization. The overall performance of a wind farm could also be increased by a rotor design with an improved efficiency that has no implications on the velocity deficit in the wake. Thus, the energy content in the wake of such a rotor is similar to the energy content of a wake forming behind rotor without improved efficiency.

The wind farm control offers large potential for the optimization of wind farms. There are mainly two approaches for wind farm control optimization, the induction based and the wake redirection control (Raach et al., 2016). A preliminary study on this topic was conducted by (Steinbuch et al., 1988) who showed that by applying control strategies the interactions between turbines can be limited and thus the energy output is maximized. A survey summarizing literature on wake farm control can be found in Knudsen et al. (2014). In a recent study Bartl and Sætran (2016) investigated the induction based control methods tip speed variation and pitch angle variation and showed that both techniques only have minor potential for wind farm optimization. Wake redirection is considered to have a bigger potential for control optimization. Fleming et al. (2015, 2014) tested the three redirection strategies yaw angle variation, tilt variation and individual pitch control. They showed good wake redirection with performance increase and load reduction for yaw and tilt variation, whereas individual pitch control resulted only in little wake redirection but an increase in blade loading. This was confirmed by Gebraad et al. (2014) who used the FLORIS model to evaluate yaw control for a small wind farm and also found a performance increase and load reduction.

In a study investigating different approaches for wind farm optimization, Fleming et al. (2016b) combined wind farm layout and wind farm control and showed that the best improvement was reached by applying a coupled control and layout optimization. This suggests, that all approaches have to be taken into account and combined to further optimize the wind farm performance. Consequently, further studies investigating wind farm layout, rotor design and wind farm control are needed.

1.1.5 Wake investigation techniques

There are mainly three techniques to investigate wind turbine wake investigations, full-scale measurements, computational fluid mechanics (CFD) simulations and wind tunnel experiments.

Full-scale experiments are widely conducted for the investigation of single turbines and wind farms. However, the measurements of full-scale wake data are rather complex, because substantial measurement equipment is needed. Nevertheless, many studies present velocity profiles measured with met masts (Barthelmie et al., 2007; Hansen et al., 2012). The installation of such met masts is expensive and thus the costs are rather high. In the last few years the development of the remote sensing technique LiDAR (laser detection and ranging) has made significant progress and LiDAR instruments have been used in several studies for wake measurements behind full-scale turbines (Kumer et al., 2015; Trujillo et al., 2016). LiDAR instruments can also be installed on the nacelle of a wind turbine to track the wake (Raach et al., 2017). However, the costs of full-scale experiments could be decreased by new full-scale measurement techniques. Such a technique was developed by Reuder et al. (2016), who equipped a drone with velocity measurement technique and used it to fly into the wake to directly measure flow properties. Notwithstanding, the biggest drawback of full-scale measurements are the uncontrollable boundary conditions. The inflow and the flow regime cannot be controlled and are constantly changing, which makes it hard to measure at defined boundary conditions and get reliable wake data. Consequently, other wake investigation techniques are needed to draw reliable conclusions on the wind turbine wake.

A 'somewhat' cheaper technique for wake investigations are numerical CFD simulations. This technique was developed intensively in the last decades and several different models were established. A state-of-the-art review on the calculation of wind turbine wake aerodynamics is presented by Sanderse et al. (2011). With computer simulations it is possible to extract detailed information of the wind turbine wake and multiple wake properties. Even though this technique is already very advanced, there are some limitations to it. Because direct numerical simulations still require too much computational capacity, small turbulent structures cannot be simulated and

numerical models are depended on different turbulence models resolving turbulence in the flow. Furthermore, boundary conditions have to be defined and the grid has to be generated. Consequently, CFD simulations are depended on various input parameters, which influence the results and thus make them unreliable. As a consequence numerical models have to be validated against reliable data obtained by measurements.

Experimental wind tunnel tests under controlled boundary conditions are good techniques to deliver reliable results for CFD validation. In the last decades several experimental studies on the wind turbine wake have been conducted. These scaled model experiments helped to better understand the wake of wind turbines and to investigate different design and operation parameters and their influence on the wake development. The wake of single turbines was investigated in detail using different measurement technique (e.g. Chamorro and Porté-Agel 2009; Medici and Alfredsson 2006). Furthermore, numerous experiments of multiple aligned turbine arrays were conducted for a better comprehension of wake interactions see amongst others (Schottler et al., 2017; Schreiber et al., 2017). Moreover, whole wind farms consisting of multiple turbine rows were investigated in the wind tunnel to better understand wind farm behavior see for example Corten et al. (2004). Even though wind tunnel experiments provide actual measurement results, there are limitations to such measurements. One disadvantage is the influence of the wind tunnel walls, which can block the flow and limit it from expanding freely. This effect gets stronger with an increasing blockage ratio, which is defined as the ratio of the wind turbine rotor and the cross-section of the wind tunnel. The biggest limitation of wind tunnel experiments is achieving scaling similarity. While it is no problem to match the tip speed ratio of a full-scale turbine it is very hard to achieve Reynolds number similarity between wind tunnel tests and full-scale applications. Only few studies, which used advanced pressurized wind tunnels, were able to achieve model Reynolds numbers, which are similar to those occurring at full-scale turbines see for example (Miller et al., 2016). Nevertheless, as pictured in Figure 1.2 low Reynolds number wind tunnel experiments provide precise measurement data, which can be used for the validation and calibration of numerical CFD simulations. The validated CFD codes in turn can then be used to predict what is happening in full-scale applications. Consequently, experimental wind tunnel studies are not only important to understand the wake structure but also to provide reference data for the validation of CFD codes.

1.2 Objective

The existing literature on wind turbine wakes indicates that a lot of studies including experimental models in wind tunnel tests, numerical simulations and measurements of

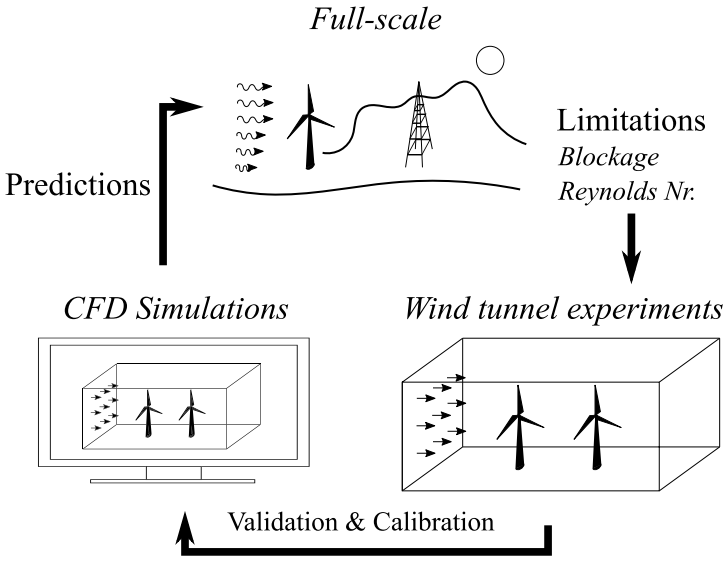

Figure 1.2: The importance of wind tunnel experiments and the connection between the three wake measurement techniques.

full-scale wind turbines have already been carried out to understand the characteristics and the behavior of wind turbine wakes. Nevertheless, there is still need for further investigation to fully understand the wake of wind turbines and thus the interaction between wind turbines.

For this PhD thesis, experimental studies were carried out to investigate the performance characteristics and the wake structures of single model wind turbines and multiple turbine arrays under various operating conditions and for different parameters that could have an effect on the wind turbine wake. The knowledge gained from this study will provide better understanding of the overall flow structure around wind turbines and the physics of rotor wake interactions and therefore help in proper planning and designing of wind farms. In addition, the generated data is used as reference for the validation of CFD codes and thus helps to improve numerical tools that are used for the simulation of wind farms.

In *Paper I*, *Paper II* and *Paper III* the focus is on rotor design and how it affects the wake development. Thus, these papers give insight on the potential of adopting the rotor design in order to improve the overall performance of a wind farm. *Paper I* focuses on how the rotor blade number is influencing the wake structure of a single wind turbine. The study should show if it could be beneficial to consider other concepts than the common three bladed turbine rotor to better account for losses due to turbine interactions. *Paper II* investigates the potential of opposite rotating rotors. Detailed measurements of the wake structure as well as the overall performance of an aligned turbine array are considered to show if different rotational directions in a wind farm

could have the potential to improve the wind farm efficiency. In *Paper III* the wake of a rotor with winglets and thus an improved efficiency is compared to that of a base line rotor. The study shall give information if a rotor, that is equipped with winglets, is changing the wake structure, and thus improving or deteriorating the performance of a wind farm.

The rotor design and winglet optimization for the winglet wake experiment in *Paper III* are presented in *Paper IV*. The goal of the study is not only the design of a rotor for the wake investigations, but also the analysis of the potential of adding winglets at the blade tips for power optimization of a single wind turbine and providing basic design instructions for further winglet concepts. Furthermore, a detailed analysis of the blade flow shall show the difference of a winglet and a baseline rotor and explain why a winglet rotor can be beneficial. Together with *Paper III* it is investigated if winglets can not only improve the efficiency of a single turbine but also a complete wind farm.

Optimizing the wind farm control by redirecting the wake with intentional yaw misalignment is the topic of *Paper V* and *Paper VI*. These studies shall help to evaluate the potential of yaw control strategies for the optimization of wind farms. Thereby, the focus of *Paper V* is on the wake structure behind yawed turbines. The paper provides detailed information about the wake structure and how it is affected by varying inflow conditions. Consequently, it provides information that is needed for the development of advanced wind farm control algorithms. *Paper VI* is focusing on the power production and loads of a turbine operating in the wake of a yawed turbine at various inflow conditions and array configurations. Together with *Paper V* this study completes the link between detailed wake flow characteristics and the performance and loads of a turbine operated in the wake.

Paper VII compares detailed experimental measurement results of complex wakes behind yawed wind turbines to numerical predictions, obtained by various CFD simulations of the same wake flow. The comparison and the analysis of discrepancies of the CFD results should help code developers to see how well their simulations perform and thus provide information for further development of CFD solvers. Furthermore, the data is published and made available to CFD developers as validation reference for CFD codes.

1.3 Thesis outline

After the introduction given in this chapter, chapter 2 describes the methods applied in the PhD thesis. Firstly, the experimental facilities and the model wind turbines that were used to study rotor wake interactions are specified. After that the different

rotor designs that were developed are introduced. The blade element momentum (BEM) code that was used for the rotor evaluation and design will be described and the 3D printing production technique, that was applied for the rotor concepts will be introduced and evaluated by comparing performance and wake measurements of aluminum and 3D printed rotors. At the end of chapter 2 the employed measurement technique and the method determining the measurement uncertainty will be explained.

In chapter 3 the results are summarized and the outcome of the articles are linked and brought in an overall perspective. A schematic summary and connection of all papers is presented in Figure 1.3. All articles can be assigned to the overall topic of the project, rotor-wake interactions. However, they are divided into the subtopics wind farm optimization and reference data for CFD validation. Whereat the major part is on the optimization of wind farms, which is again divided into the two categories rotor design and control strategies. Within the topic of rotor design the three topics, which are, comparison 2-3-bladed rotors (*Paper I*), counter rotating wind turbine rotors (*Paper II*) and winglet rotors (*Paper III* and *Paper IV*) are discussed. Within control strategies the focus is on intentional yaw misalignment (*Paper V* and *Paper VI*). The topic reference data for CFD validation is represented by *Paper VII*, which is based on the wind turbine wakes in yaw measurement campaign. This article is complementing the studies for wind farm optimization by comparing the experimental results to numerical CFD predictions and providing detailed data that can be used by CFD developers for the validation of their numerical wake simulation codes. The motivation for all investigated topics will be summarized, before the literature will be briefly reviewed. Furthermore, the major results of each study will be summarized and a conclusion on their potential for wind farm optimization will be given.

The introductory chapters of the PhD thesis will be completed by the conclusions, in which the potential for wind farm optimization of the different approaches will be analyzed. Furthermore, recommendations for future research work on the promising methods for wind farm optimization will be given.

After the introductory chapters, all the papers that are part of the PhD project will be provided. The seven articles are ordered regarding the research topics and will not be assorted in a chronological order.

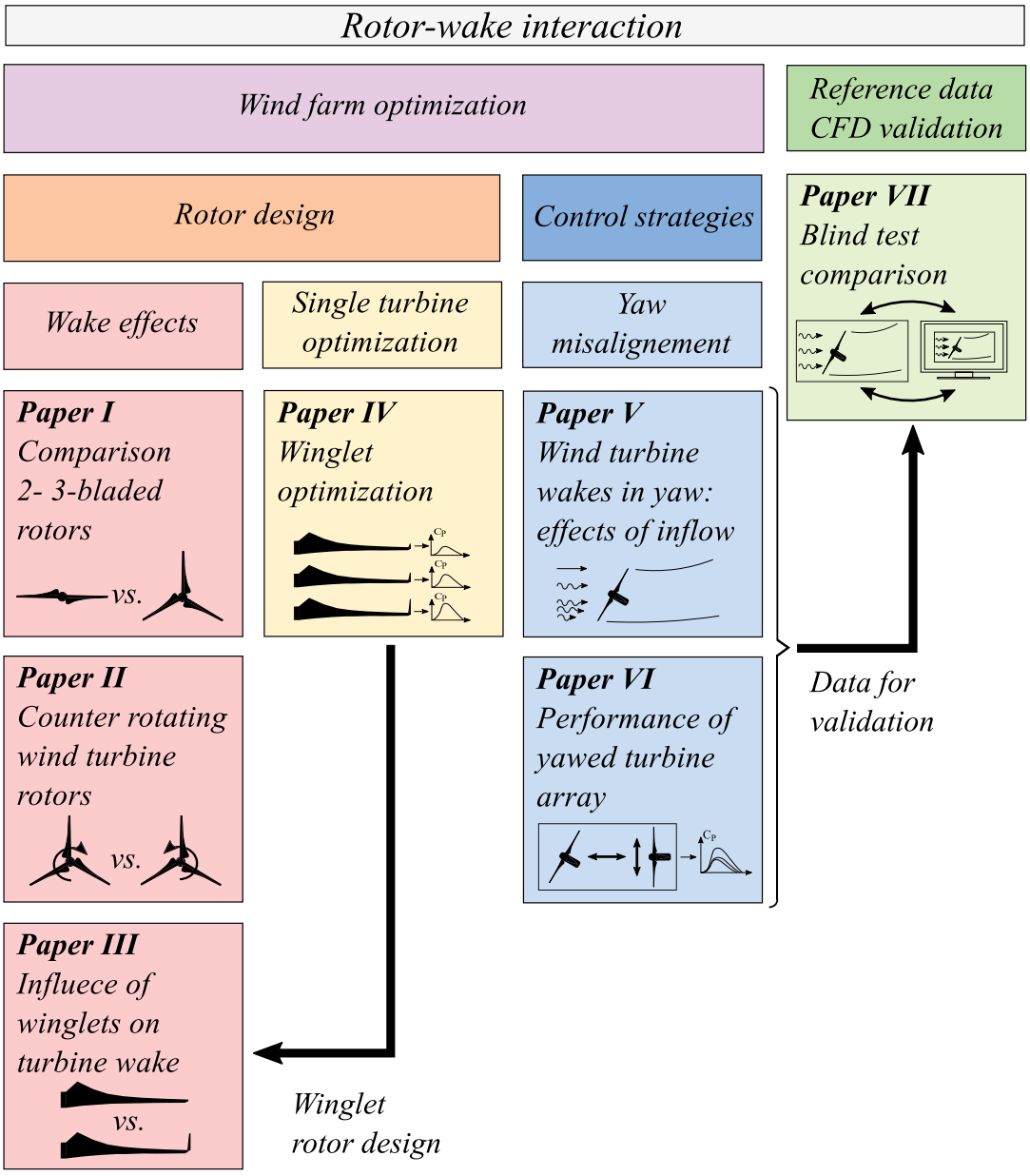

Figure 1.3: Summary and connection of all papers in the thesis.

Chapter 2

Methodology

This chapter introduces the methodologies applied in the PhD study. First the wind tunnel is described and different inflow conditions with varying velocity distribution and turbulence levels are introduced. Then the three model wind turbines used for the experiments are presented. Next the focus is on the design of the different model rotors. The blade element momentum (BEM) method, which was used for the design of the blades and the numerical investigation of the rotors, will be briefly summarized. Furthermore, the different rotor concepts, used in the various experiments will be presented. Because the new rotors were manufactured with the 3D printing technique, it will be analyzed whether 3D printed rotors are applicable in wind tunnel tests. Then the measurement technique, which was used to measure the power, force and wake properties is introduced. The chapter is concluded with a description of the method that was used to quantify the measurement uncertainty and presentation of typical measurement uncertainties occurring during the project.

2.1 Wind tunnel

All the experimental studies were conducted in the closed-loop wind tunnel in the Fluid Mechanics Laboratory at the Norwegian University of Science and Technology (NTNU). The test section of the wind tunnel has a length of 11.15 m and a width of 2.71 m, it is depicted in Figure 2.1. The roof of the wind tunnel was adjusted for zero pressure gradient and thus the height increased from 1.80 m at the inlet to 1.85 m at the outlet. The tunnel is driven by a radial fan with a power of 220 kW, at the end of the test section. The test section inlet is formed as a contraction nozzle with static pressure taps all around the circumference of the nozzle inlet and outlet cross-section measuring the pressure difference Δp. Applying the continuity equation and Bernoulli's

law, Δp can be used for calculating the inlet velocity of the wind tunnel with:

$$U_\infty = \sqrt{\frac{2\Delta p}{\rho\left(1-\frac{A_{out}^2}{A_{in}^2}\right)}}, \tag{2.1}$$

where ρ is the air density, A_{in} the area of the nozzle inlet and A_{out} the area of the nozzle outlet. The advantage of this measurement technique is, that no device is blocking the flow and thus the inlet velocity U_∞ can be obtained without disturbing the flow. In all experiments conducted for the seven papers the inlet velocity of the wind tunnel was adjusted to $U_\infty = 10.0$ m/s.

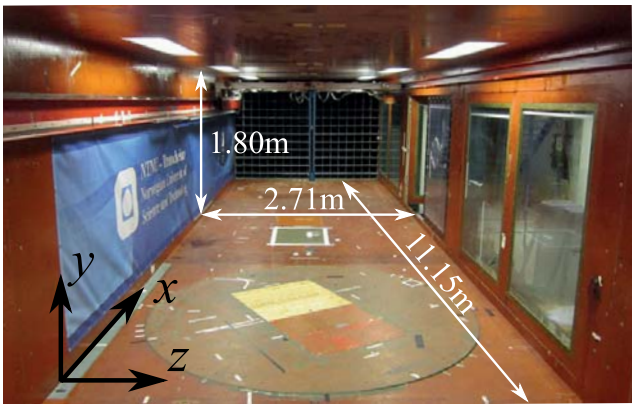

Figure 2.1: Test section of the wind tunnel with dimensions and coordinate system, looking in flow direction.

2.1.1 Inflow conditions

During the experiments three different inflow conditions were investigated: low-turbulence uniform, high-turbulence uniform and high-turbulence shear. The higher turbulence was generated by passive grids at the test section inlet. Figure 4 shows the grid setting at the inlet and the normalized velocity $U_\infty^* = {}^{\bar{u}}/_{U_{ref}}$ and turbulence intensity $TI = {}^{u'}/_{U_{ref}}$ at the turbine position, which is $2D$ behind the grid. Where U_{ref} is the reference velocity at hub height, $\bar{u}$ is the time averaged velocity and u' the turbulent velocity component.

Low-turbulence inflow

The low-turbulence inflow was applied in most studies and was therefore investigated in all Papers except *Paper VII*. As pictured in Figure 4a there was no grid installed at the inlet of the test sections resulting in a flow with only marginal turbulence intensity of $TI = 0.23\%$. TI and U_∞ are uniformly distributed in the empty wind tunnel

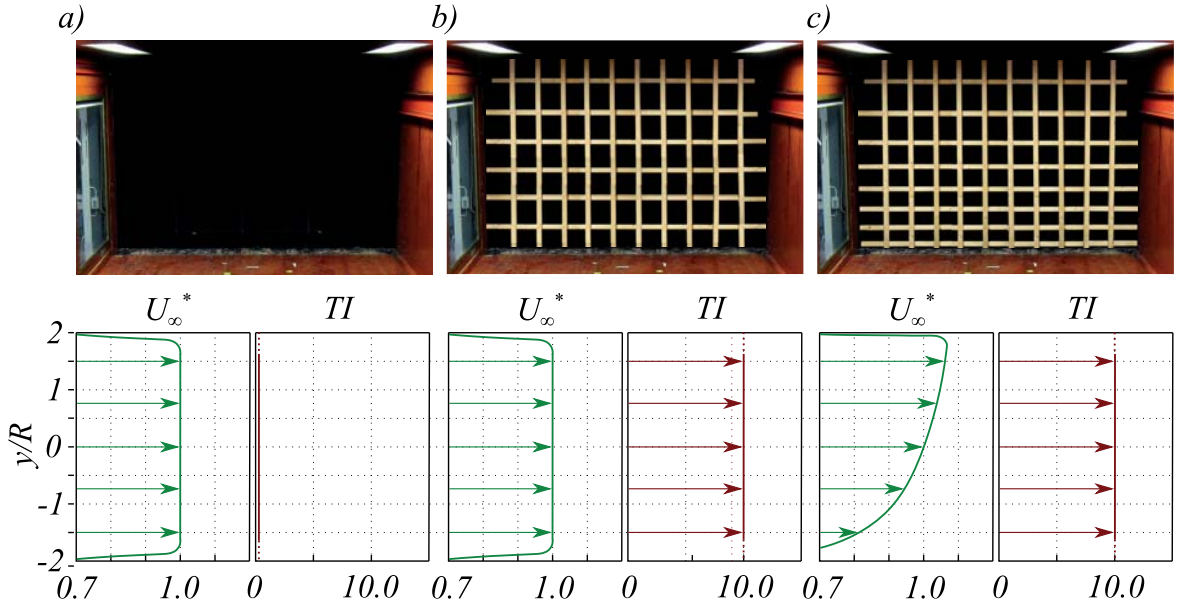

Figure 2.2: Different inlet configurations and resulting $U_\infty{}^*$ and TI in [%] at the turbine position for (a) low-turbulence uniform, (b) high-turbulence uniform and (c) high-turbulence shear inflow.

and the mean velocity over the rotor swept area is found to deviate by ±0.8% for $U_\infty = 10.0$ m/s.

High-turbulence inflow

The high-turbulence inflow was used in *Paper IV*, *Paper V*, *Paper VI* and *Paper VII*. In order to get a uniform high-turbulent flow the inlet was equipped with a turbulence grid as shown in Figure 4b. The grid is fabricated from evenly spaced wooden bars with a clearance of 0.24 m resulting in a solidity of 35%. The grid generates a turbulence intensity of $TI = 10.0\%$ at the turbine position ($0D$). However, because the turbulence is only generated at the inlet it decays with increasing distance resulting in $TI = 5.5\%$ $3D$ and $TI = 4.1\%$ $6D$ behind the turbine position, detailed measurements of U_∞ and TI are presented in *Paper V*. The grid structure can still be observed in the flow at the turbine position, resulting in a spatial variation of U_∞ over the rotor area of ±2.5% at the turbine position. However this variation is found to be only ±1.0%, $3D$ behind the turbine.

High-turbulence shear inflow

The third inflow condition is a high-turbulence shear flow that was used in *Paper V* and *Paper VII*. The grid generating the turbulent shear flow is shown in Figure 4c. It has a solidity of 38% and is also made of wooden bars that are distributed evenly

in horizontal direction with a clearance of 0.24 m. In vertical direction however, the distance between the bars is increasing from 0.016 m at the wind tunnel floor to 0.30 m at the ceiling. This arrangement is resulting in a velocity shear in which the normalized velocity is 1.0 at hub height, see Figure 4c. The shear profile can be described with the power law:

$$\frac{\bar{u}}{U_{ref}} = \left(\frac{y}{y_{ref}}\right)^{\alpha}. \tag{2.2}$$

Equation (2.2) describes the mean wind speed $\bar{u}$ as a function of height y provided that U_{ref} is known at a reference height y_{ref}. The power law coefficient α determines the strength of the shear. The described grid was designed to obtain a α of 0.11, which corresponds to a neutral atmospheric boundary layer (Wharton and Lundquist, 2012). The turbulence intensity at the turbine position is $TI = 10.0\%$ at hub height and with increasing distance it decays similar to that of the high-turbulence grid, the detailed streamwise evolution is shown in *Paper V*.

2.1.2 Wind tunnel blockage

As already mentioned in Chapter 1, a limitation in wind tunnel experiments is the blockage effect. The model wind turbines are an obstacle in the flow, consequently part of the flow is evading the rotor and expanding around the turbine. If the cross-section fraction that is blocked by the wind turbine rotor is too large, the expansion is limited by the wind tunnel boundaries and the flow hitting the turbine is influenced, resulting in higher velocities at the turbine. The model rotors used in the study have a blockage ratio of approximately 13% in the NTNU wind tunnel. Sarlak et al. (2016) showed in their study that a blockage ratio of this size has already an influence on the power and thrust measurements of the turbine. There exist different methods correcting for the wind tunnel blockage, see for example (Chen and Liou, 2011; Ryi et al., 2015). Nevertheless, they are also based on different assumptions. Consequently, analyzing the results of wind tunnel experiments it has to be kept in mind that the power and forces of a turbine could be higher in comparison with the free flow condition.

2.2 Model wind turbines

The three model turbines Turbine 1 (T1), Turbine 2 (T2) and Laterally Angled Rotating System 1 (LARS1), which were used in the wind tunnel experiments, are shown in Figure 1. Detailed technical drawings of the model turbines are attached in Appendix A. The turbines were already used for various studies at NTNU. Krogstad and Lund

(2012) designed the standard NTNU rotor and measured power and thrust for the single turbine T2. This study was extended by Adaramola and Krogstad (2011) who investigated the performance of an aligned turbine array with turbines T1 and T2 at various separation distances, yaw angles and blade pitch angles. The first wind turbine wake measurements at NTNU were conducted by Krogstad and Adaramola (2012) who investigated the near wake of the single turbine T2 at different tip speed ratios and yaw angles. Moreover, measurements of the wake formed behind a turbine array of T1 and T2 were conducted by Bartl et al. (2012) and Schümann et al. (2013). A recent study by Pierella and Sætran (2017) examined the influence of the tower structure on the wake development behind the single turbine T2 and an aligned array with T1 and T2. Furthermore, an elaborated analysis, providing detailed information about the wake behind single turbine T2 was performed by Eriksen and Krogstad (2017a,b).

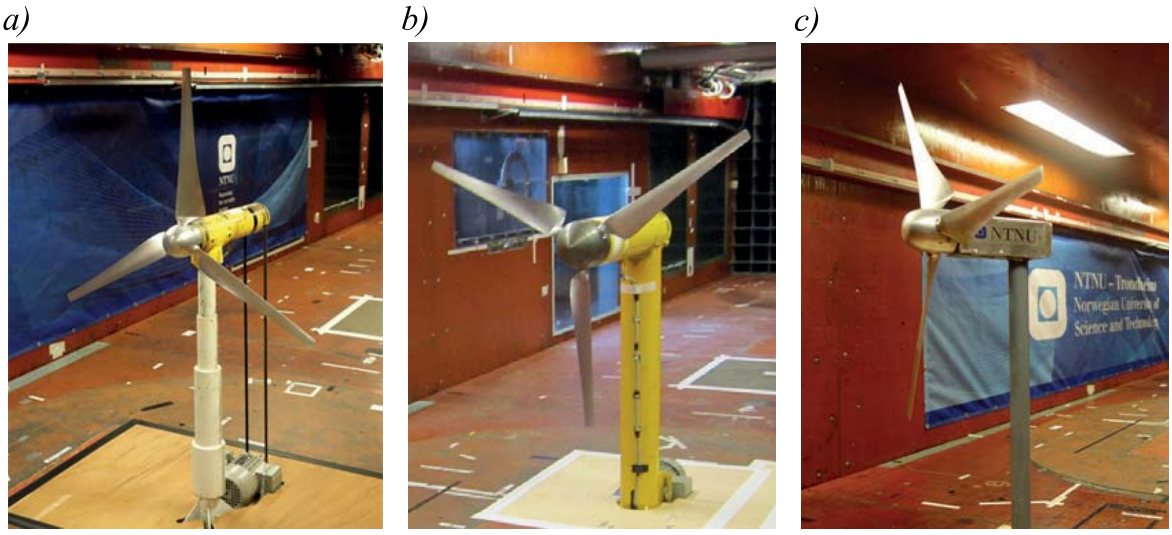

Figure 2.3: Model wind turbines (a) T2, (b) T1 and (c) LARS1, all equipped with the standard 3-bladed NTNU rotor.

The turbines T1 and T2 are driven by an asynchronous motor that is located at the base of the turbine tower and controlled by a frequency converter. This configuration enables an adjustment of the turbines rotational speed, independent from the flow regime in the wind tunnel. Consequently, the turbines can be operated at a wide range of tip speed ratios even though they operate in stall. Model turbine T2 was the most common turbine in the PhD study and was used in all papers except *Paper V*. On the contrary T1 was only used as a downstream turbine in *Paper II*. Model turbine LARS1 was designed for the yaw experiments and is employed in *Paper V*, *Paper VI* and *Paper VII*. It has a slimmer tower and a smaller nacelle as turbines T1 and T2 to limit blockage of the wake flow when the turbine is yawed. It is driven by a servo motor that is installed inside the turbine nacelle. The motor is also frequency-controlled

enabling operation at a constant rotational speed. The three turbines have a similar hub structure so that all different rotors can be installed on all turbines. During the yaw experiments another model wind turbine, from ForWind in Oldenburg (Germany) was used. The turbine is somewhat smaller than the NTNU turbines. A detailed description is presented in (Schottler et al., 2016a). Wake measurements behind this turbine are part of *Paper VII*.

2.3 Model rotor design

For the PhD work the existing rotors at NTNU were used in addition to a new set of model rotors, which were designed in the course of this study. The two parameters that have to be determined in the blade design are the span-wise chord length c and twist angle θ distribution. The determination of these parameters is based on different approaches for the diverse blade designs. The classical blade element momentum (BEM) theory was applied to evaluate the rotor designs. Furthermore, it was used in the rotor design process together with another technique, which is based on the modification of existing rotor designs. In the following sub-chapters, the BEM method is explained, the different rotors are described and their design and production process are discussed.

2.3.1 Blade element momentum method

For the evaluation of the different rotors and the blade design, a classical BEM code was developed, which is described below based on (Hansen, 2015). Furthermore, non-dimensional numbers, which are important for the evaluation of wind turbine rotors will be explained.

The available energy for a wind turbine is defined by the kinetic energy of the wind. It is given by:

$$P_{avl} = \frac{1}{2}\rho A_R U_\infty^3, \tag{2.3}$$

where A_R is the rotor swept area However, the turbine cannot extract all the available power from the wind. The power coefficient C_P is a dimensionless number, which describes the aerodynamic efficiency of a wind turbine and thus, the amount of energy it is extracting from the flow:

$$C_P = \frac{P}{0.5\rho A_R U_\infty^3}. \tag{2.4}$$

P denotes the power extracted by the rotor. The maximum aerodynamic efficiency of a wind turbine according to Betz is $C_{P,Betz} = \frac{16}{27}$. Similar to the power coefficient another dimensionless number, the thrust coefficient C_T can be calculated with:

$$C_T = \frac{T}{0.5\rho A_R U_\infty^2}, \tag{2.5}$$

where T is the thrust force acting on the rotor. C_T is not directly related to the aerodynamic efficiency. However, it is an indication on how much the flow is affected by the wind turbine. Another important non-dimensional parameter is the tip speed ratio λ, which is defined as the ratio of the blade tip speed and the inflow velocity,

$$\lambda = \frac{\omega R}{U_\infty}, \tag{2.6}$$

where ω is the rotational speed and R is the rotor radius.

Flow around wind turbine

The stream tube, pictured in Figure 2.4 is a common one-dimensional approach to describe the flow around a wind turbine. It can be seen, that the velocity is already decreasing before hitting the turbine. This reduction in velocity can be described by a rotor induced axial velocity component acting in opposite flow direction, which is defined by the axial induction factor a. With the axial induction factor, the axial velocity u_1 at the rotor plane can be expressed with the known inflow velocity U_∞, which becomes important when calculating the aerodynamics at the rotor blades:

$$u_1 = (1 - a)U_\infty. \tag{2.7}$$

Considering the three-dimensionality of the flow, the rotating rotor blades cause wake rotation behind the wind turbine, which induces additional tangential velocity. This additional tangential velocity component in the wake can be specified with the tangential induction factor a'. Similar to the axial velocity, the tangential velocity at the rotor plane can be calculated by:

$$u_t = (1 + a')\omega r. \tag{2.8}$$

where r is the radial position of the blade element. Opposite to the axially induced velocity the tangentially induced velocity is added to the rotational component as the flow is accelerated in tangential direction.

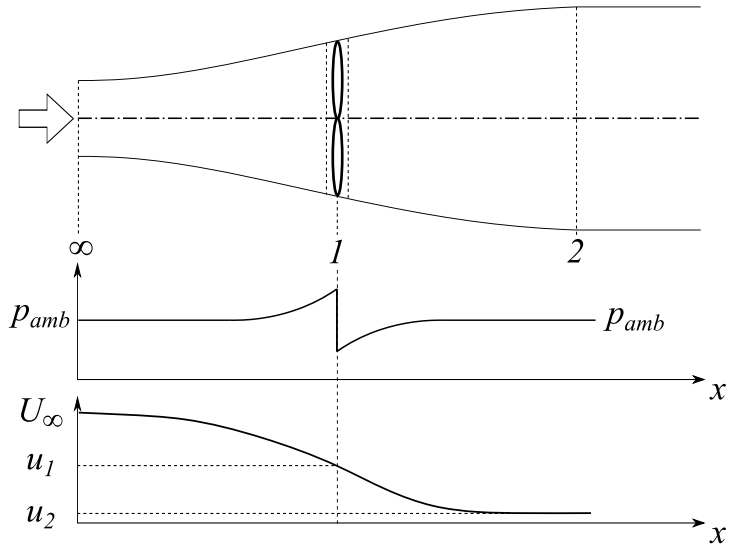

Figure 2.4: Schematic stream tube describing the one-dimensional flow passing a wind turbine, with the corresponding pressure and velocity distribution.

Rotor evaluation with BEM method

In the blade element momentum method, the stream tube, presented in Figure 2.4 is divided into several rings. As a result the flow regime at each blade element can be analyzed (see Figure 2.5) and the steady-state power and thrust of the rotor can be calculated. The BEM method is a two-dimensional approach, consequently the span wise velocity component is not considered and thus each element is independent and there is no lateral transfer between the elements, which depicts a limitation of the method.

The flow regime on a blade element and the resulting forces are pictured in Figure 2.5. It can be seen that the velocity acting on the blade element V_{rel} is the resulting velocity from the axial and tangential velocity component, which stem from the wind speed and the rotor rotation respectively. The flow angle φ is defined as the angle included between V_{rel} and the rotor plane, it can be calculated along with the induction factors by applying:

$$\varphi = \tan^{-1}\left(\frac{(1-a)U_\infty}{(1+a')\omega r}\right). \tag{2.9}$$

The flow angle is split into the twist angle of the blade θ and the angle of attack α_a, resulting in:

$$\alpha_a = \varphi - \theta. \tag{2.10}$$

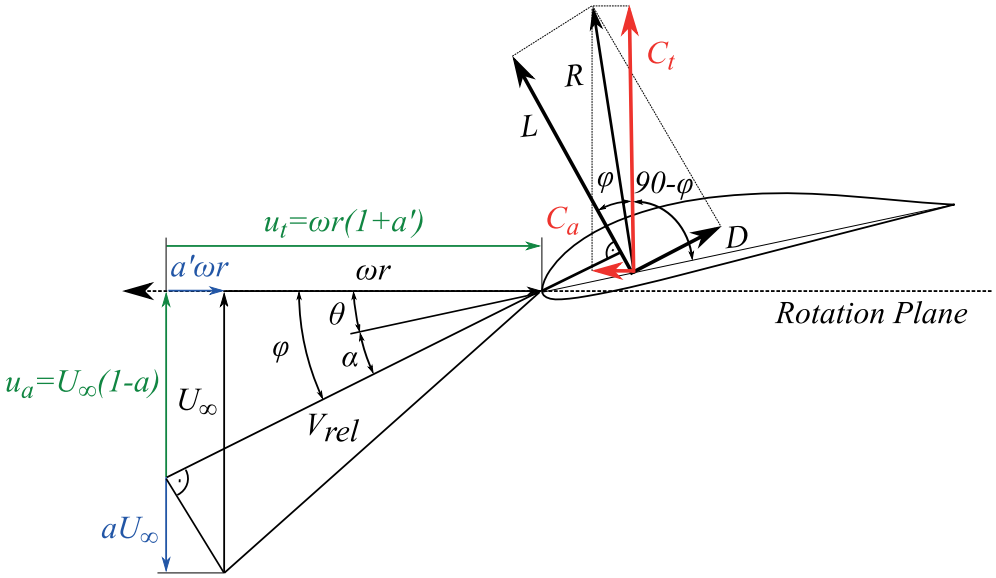

Figure 2.5: Blade element with velocity triangle at the rotor plane and the resulting force R, with components for lift L and drag D and the load coefficients in axial and tangential direction.

The lift and drag coefficients C_L and C_D, which are non-dimensional coefficients representing the lift and drag force acting on the blade element, can be found in look up tables, simulated or obtained through experiments. In this study C_L and C_D were calculated using the program XFOIL (Drela, 1989). With this two dimensionless parameters the axial and tangential load coefficients C_a and C_t can be calculated according to:

$$C_a = C_L \cos\varphi + C_D \sin\varphi, \tag{2.11}$$

and

$$C_t = C_L \sin\varphi - C_D \cos\varphi. \tag{2.12}$$

The evaluation process with the BEM code is iterative as the induction factors are unknown in the beginning. So, in the BEM analysis initial values for the induction factors a and a' need to be guessed, as they are necessary to calculate the flow angle. After the load coefficients are obtained, the actual induction factors can be calculated according to:

$$a = \frac{1}{\frac{4F\sin^2\varphi}{\sigma_s C_a} + 1}, \tag{2.13}$$

and

$$a' = \frac{1}{\frac{4F \sin\varphi \cos\varphi}{\sigma_s C_t} - 1}. \tag{2.14}$$

F denotes the Prandtl's tip loss factor, which corrects the induction factors for a finite blade number and the spanwise flow, limiting the loads at the tip, consequently, its effect is increasing with increasing radial position r. σ_s is the solidity, which is defined as the fraction of the annular area that is covered by the blades. Furthermore, in the BEM code values of $a > 0.2$ need to be corrected according to Glauert to account for the fact that the thrust forces can be bigger as the static pressure in the flow. If the initial induction factors and the actual induction factors are within a defined tolerance level, the iteration is stopped and the thrust and torque of each blade element are calculated with:

$$T_{(r)} = \frac{1}{2}\rho B \frac{U_\infty^2 (1-a)^2}{\sin^2\varphi} c C_t \Delta r, \tag{2.15}$$

and

$$M_{(r)} = \frac{1}{2}\rho B \frac{U_\infty (1-a)\omega r (1+a')}{\sin\varphi \cos\varphi} c C_t r \Delta r, \tag{2.16}$$

where, c is the chord length of the blade element B is the number of rotor blades and Δr is the blade element length in radial direction. The total power of the rotor P is the sum of the shaft torques from all annual sections:

$$P = \sum M_{(r)} \omega r. \tag{2.17}$$

Similar to the torque the thrust force acting on the rotors is the sum of the thrust forces of all blade elements:

$$P = \sum T_{(r)}. \tag{2.18}$$

BEM for blade design

For the blade design the chord length and twist angle were determined for each blade element. Therefore, the axial induction factor was optimized according to:

$$16a^3 - 24a^2 + a(9 - 3x^2) - 1 + \lambda_{loc}^2 = 0, \tag{2.19}$$

where $\lambda_{loc} = \frac{\omega r}{U_\infty}$ is the local tip speed ratio. The corresponding tangential induction factor is dependent on the axial induction factor and could thus be calculated by:

$$a' = \frac{1 - 3a}{4a - 1}. \tag{2.20}$$

The flow angle was obtained by solving Equation (2.9) and together with the optimum angle of attack of the used airfoil $\alpha_{a,opt}$ the twist angle was calculated according to:

$$\theta = \varphi - \alpha_{a,opt}. \tag{2.21}$$

The chord length for each blade element could then be obtained by:

$$c = \frac{8\pi a \lambda_{loc} \sin^2\theta R}{(1 - a) B C_a \lambda}. \tag{2.22}$$

The results for the separate blade elements together with the radial position resulted in the chord length and twist angle distribution of the new blade.

2.3.2 Rotors

In order to investigate the influence of the rotor design on the wake development, several rotors were tested in the wind tunnel experiments. The chord and twist distribution of these rotors is presented in Figure 2.6 and the key parameters are summarized in Table 2.1.

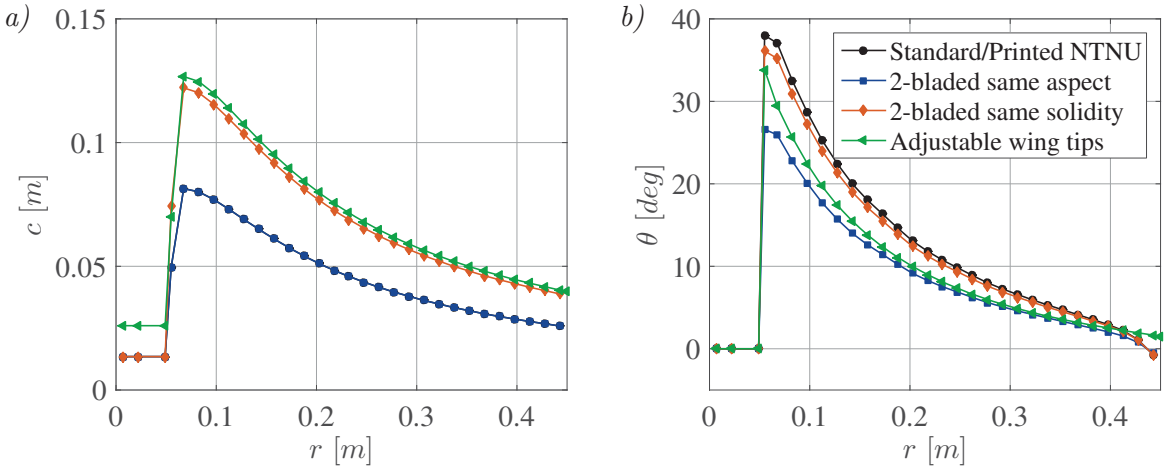

Figure 2.6: Span-wise (a) chord length c and (b) twist angle θ distribution for the rotors used in the PhD study (r is the radial position).

The existing rotors at NTNU were milled from an aluminum alloy. Such rotors are very precise and sturdy and are suited very well for wind tunnel experiments.

Table 2.1: Key parameters of the rotors used in the PhD study, (tip speed ratio (λ) clock-wise (CW) and counter-clock-wise (CCW) rotation).

Rotor	Number blades	opt. λ	C_P	C_T	Rotational direction	Airfoil	Material	Papers
Standard NTNU	3	6	0.46	0.90	CCW	S826	Aluminum	*II*, *V*, *VI*, *VII*
Printed NTNU	3	6	0.48	1.00	CW	S826	VeroGray	*I*, *II*
2-bladed same solidity	2	6	0.45	0.98	CW	S826	VeroGray	*I*
2-bladed same aspect	2	7	0.45	1.03	CW	S826	VeroGray	*I*
Adjustable wing tips	2	6	0.47-0.52	0.97-1.08	CCW	R-opt	VeroGray	*III*, *IV*

However, this production technique is very costly and could therefore not be considered as production method for the various model rotors. Therefore, another technique was selected and the rotors were produced using a considerably more reasonable manufacturing option of rapid prototyping using a 3D printer. The printer used for the blade fabrication is a Objet Eden 500V that works based on the Multi-Jet Modeling technique. This technique enables the production of very detailed parts with a high accuracy and smooth surfaces. Accordingly the fabricated blades are of high quality and their appearance is similar to the milled aluminum blades. Nevertheless, they were manufactured from a material called VeroGray, which has worse performance than aluminum regarding tensile strength and modulus of elasticity (Ver, 2016). Accordingly, they act different in the wind tunnel test. Therefore, their applicability in wind tunnel tests was verified and evaluated in 2.3.3.

Standard NTNU rotor

The standard NTNU rotor (see Figure 1) was used in most studies of the PhD study and it additionally served as reference for all the other rotor designs. The blades for the rotor were designed using BEM theory, the design and the rotor are described in detail in (Krogstad and Lund, 2012). The rotor has a diameter of $D = 0.984$ m and has three blades, which are fabricated from aluminum. Therefore, it is well suited for wind tunnel experiments as the blades do not deflect and thus have a defined geometry even when operated under heavy load. The rotor is based on the NREL S826 airfoil

from root to tip. The shape of the airfoil is pictured in Figure 2.7 and its polars for $Re = 1.0{\cdot}10^5$ are presented in Figure 2.8. A detailed description of the airfoil can be found in (Somers, 2005).

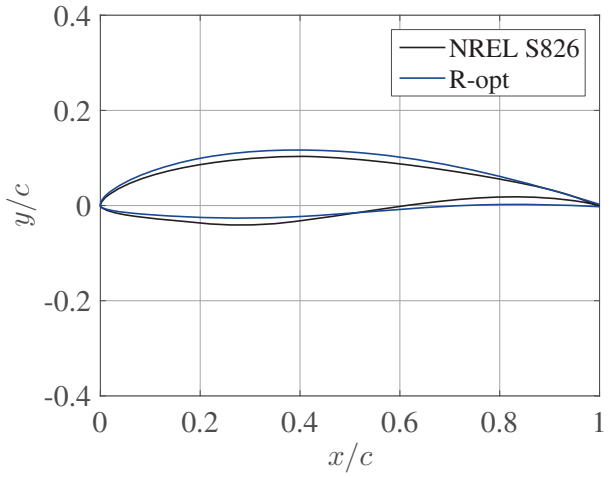

Figure 2.7: Airfoil shapes used for the model rotors.

The airfoil was originally developed as tip airfoil for full-scale wind turbines, hence it was designed for Reynolds numbers of $Re \approx 1.0{\cdot}10^6$. This is approximately one magnitude higher as the chord based Reynolds number at the blade tip in the experiments, which is approximately $Re_{c,tip} = 1.1{\cdot}10^5$ at the optimal tip speed ratio of the rotor ($\lambda = 6$) and the inlet velocity of $U_\infty = 10.0\,\mathrm{m/s}$. However, Krogstad and Lund (2012) performed a Re dependence test and found a performance independence for $U_\infty > 9.0\,\mathrm{m/s}$. Consequently, the airfoil performs already decently at lower Re. The airfoil polars for $Re = 1.0{\cdot}10^5$ generated by XFoil are presented in Figure 2.8 . This rotor was used in the experiments for *Paper II Paper V Paper VI* and *Paper VII*.

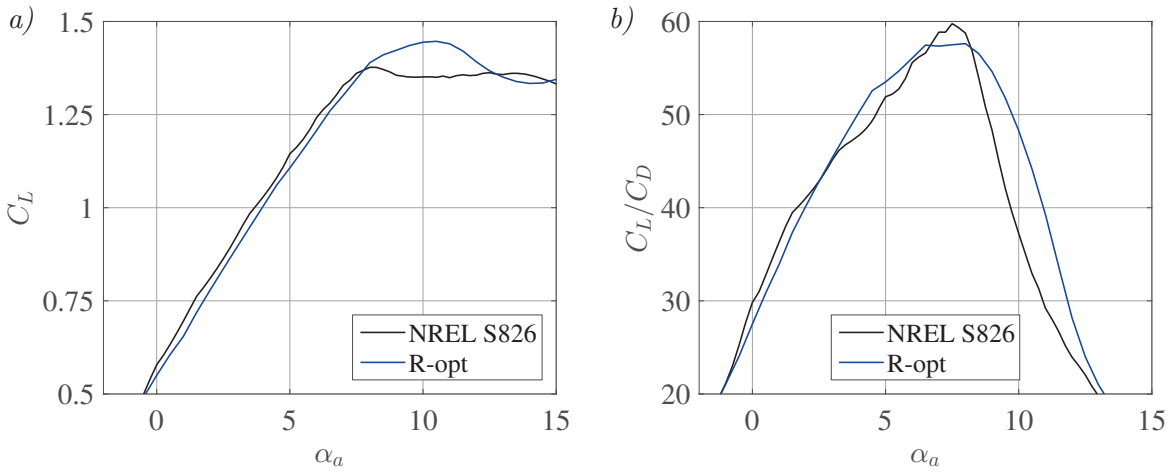

Figure 2.8: Predicted airfoil polars at $Re = 1.0{\cdot}10^5$ using XFOIL.

2-bladed rotors

For *Paper I* the effect of the blade number on the wake development was investigated. Accordingly new 2-bladed rotors were designed, they can be seen in Figure 2.9. The goal of the design was to obtain 2-bladed rotors that have similar performance as the 3-bladed reference rotor, which is the standard NTNU rotor. To get rotors with similar C_P and C_T, the chord and twist distribution of the blades from the standard NTNU rotor were modified. To find designs with matching C_P and C_T, the newly designed blades were evaluated with a BEM code .

Figure 2.9: Model rotors for the experiment comparing the effect of the blade number on the wake development, mounted on model turbine T2 (taken from *Paper I*).

For the 2-bladed rotors, two design approaches, which have the same aspect ratio and same solidity were considered. For the rotor with the same blade aspect ratio the chord length distribution is similar to the 3-bladed rotor and the twist distribution was modified until the maximum C_P's of the 2-bladed rotors match that of the 3-bladed reference rotor. This results in a rotor blade that has twist angles that are 70% of those of the reference blades (see Figure 2.6). The 2-bladed rotor with the same solidity as the 3-bladed rotor, has blades with chord lengths that are 1.5 times greater as those of the reference blade. Moreover, the BEM analysis yielded in a slightly modified twist distribution that is 95% of those of the reference blade (see Figure 2.6). The three rotors that were manufactured with the 3D printing technology and tested in the study are shown in Figure 2.9. Because they all rotate in clockwise direction, the printed 3-bladed rotor together with the standard NTNU rotor were also used for the counter rotation experiment investigated for *Paper II*.

Rotor with adjustable wing tips

In *Paper III* and *Paper IV*, the effect of winglets on the rotor performance and the wake are investigated. Therefore, a new rotor with exchangeable wingtips was developed. As it can be seen in Figure 2.10, the last 0.05 m of the blade tip can be changed. In this way different tip winglet shapes can be investigated with the model rotor. The rotor has two blades because the chord length and thus the thickness of the profile could be designed bigger than for a 3-bladed rotor. This thicker profile was needed because of constructional constraints, as the wing tip needs to be attached to the blade with a threaded rod that runs through the whole blade. Furthermore, the stability of the blade could be increased by thicker profiles and thus the deflection of the blade tips under operation would be limited. This was considered to be very important, since the experimental measurement results were used for validation of a CFD code for the winglet optimization.

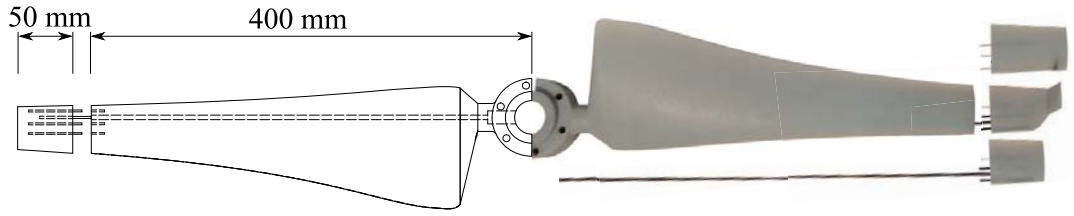

Figure 2.10: Model wind turbine rotor with exchangeable blade tips.

To further increase the stability of the blade in the tip region a new airfoil named R-opt was designed. As it can be seen in Figure 2.7, the R-opt profile is thicker than the S826 in the trailing edge region to limit torsion of the blade. The airfoil was optimized for $Re = 1.0{\cdot}10^5$ and therefore has a better performance at this Reynolds number as the S826 airfoil (see Figure 2.8).

2.3.3 3D printed blades for wind tunnel tests

The milled NTNU rotors and the 3D printed rotors used in the PhD study are fabricated from different materials with diverse properties, see Table 2.2. Therefore, they perform slightly different in the wind tunnel tests. While the Aluminum rotor is stiff and not deforming at all, the 3D printed blades deflect with increasing aerodynamic forces. To quantify this effect and to see if the 3D printed blades are applicable in the wind tunnel test, the performance and rotor forces of two identical 3-bladed rotors, one milled from Aluminum and one 3D printed in VeroGray were investigated and compared.

The power coefficient C_P over a range of λ is pictured in Figure 2.11a. It can be seen that the two curves slightly diverge and the printed rotor has a somewhat better performance. However, the differences up to $\lambda = 7.0$ are only insignificant and are

Table 2.2: Relevant mechanical properties of blade materials Aluminum and VeroGray.

Material	Tensile strength [N/mm^2]	Modulus of Elasticity [N/mm^2]	Density [kg/m^3]
Aluminum	∼250	70,000	2.7
VeroGray	60	3,000	1.17

within the measurement uncertainty. However, when $\lambda > 7.0$ the discrepancy of the graphs is increasing, resulting in a higher run-off tip speed ratio for the 3D printed rotor.

A similar trend can be observed for the thrust coefficient C_T, shown in Figure 2.11b. Whereas the graphs for C_T are almost identical until $\lambda = 7.0$, they start diverging from there increasingly. While the forces on the Aluminum rotor are getting bigger with increasing λ, the forces on the 3D printed rotor are not increasing as strongly and even start to decrease from $\lambda = 10.0$.

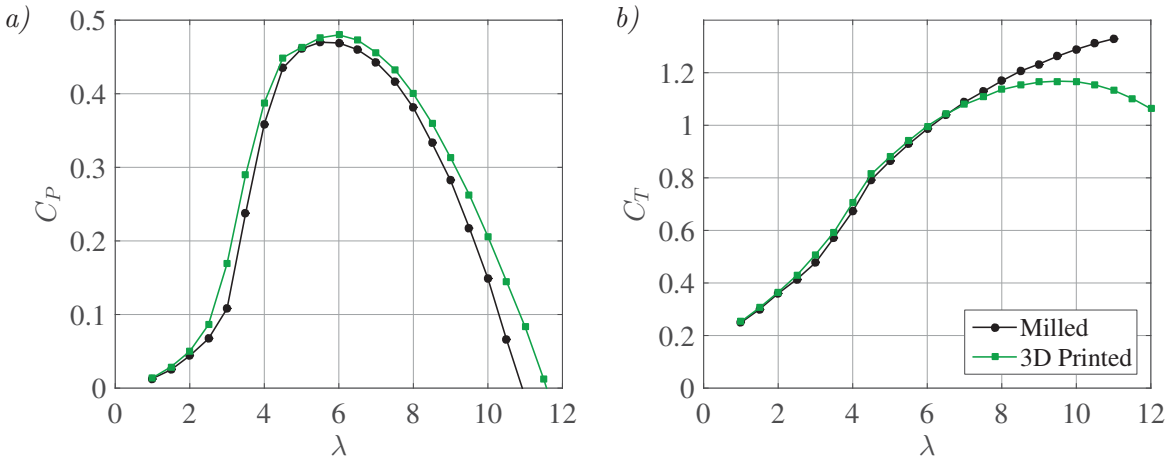

Figure 2.11: (a) C_P and (b) C_T for the 3-bladed rotor milled from Aluminum and 3D printed in VeroGray.

The difference in performance can be explained by the blade deformation of the 3D printed rotor, which is pictured for $\lambda = 6.0$ and $\lambda = 10.0$ in Figure 2.12. The blade deformation was determined with an optical method. The blade tip was illuminated by a stroboscopic flash light that was synchronized with the rotational speed of the turbine. Using this method the airfoil shape could be frozen and pictures of the deformed blade were recorded with a camera on a fixed tripod. An computational evaluation of the images resulted in the values for the deflection and twist of the blade at the tip. At the optimal tip speed ratio of $\lambda = 6.0$, the blade tip is clearly deflected backwards. However, the blade is just shifted backwards, which is expected to have no decisive influence on

the rotor performance, as C_P and C_T are alike at $\lambda = 6.0$. A different deformation can be observed at $\lambda = 10.0$, where the printed blades are not only deflected backward but also slightly twisted in clock-wise direction. This additional twist angle changes the flow regime over the blade and thus, has a significant influence on the rotor performance, which is due to the strongly decreasing C_L/C_D for low α_a (see Figure 2.8a). The effect can be seen in the distinct differences in C_P and C_T between the Aluminum and 3D printed rotor at $\lambda = 10.0$.

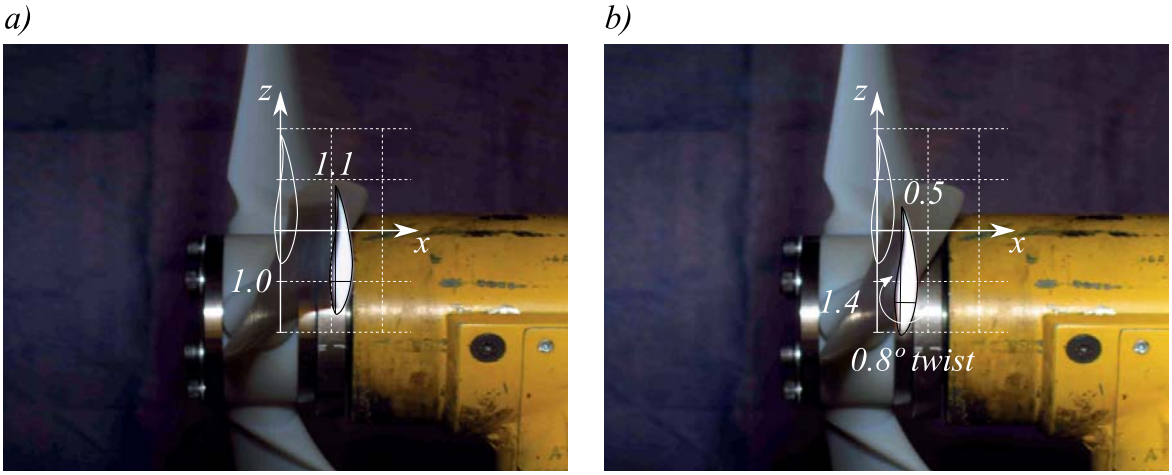

Figure 2.12: Deformation of the blade tip of the 3D printed 3-bladed rotor for $U_\infty = 10.0$ m/s at (a) $\lambda = 6$ and (b) $\lambda = 10$. With the blade deflection in x- and y-direction given in cm.

The significant differences between the two rotors are caused by a twist of the blade tip that occurs at tip speed ratios, which are beyond the optimum tip speed ratio. Therefore, it can be concluded that the printed rotors are well suited for wake investigations carried out at the optimum tip speed ratio of the rotor. However, measurement results at high tip speed ratios have to be treated with special caution. This also applies for results that should be used as reference data for CFD validation. For such experiments Aluminum rotors are favored as they do not deform and have defined geometrical properties, also at high tip speed ratios.

2.3.4 Scaling effects

The scaling of the model rotors is another limitation of wind tunnel tests. Whereas the model turbines are operated to match tip speed ratios of full scale turbines, it is almost impossible to match the chord based Reynolds number at the tip, which is calculated by:

$$\mathrm{Re} = \frac{V_{rel} c}{\nu}, \tag{2.23}$$

where ν is the kinematic viscosity of air. The viscosity and and the relative velocity V_{rel} in the model-scale and in full-scale are identical, but the chord length c is significantly different resulting in model Reynolds numbers which are around one magnitude lower as those appearing on full-scale turbines.

Even though, the the Reynolds number cannot be matched, the polars of the used airfoil should be stable in the operational range of the rotor. This is important because the Reynolds number is not a constant value, but can change along the blade in the course of one rotation. Consequently, if the airfoil polars are not stable for the occurring *Re*, the axial and tangential blade forces can alter for parts of the blade where extreme Reynolds numbers occur.

As discussed in section 2.3.2, the NTNU rotor was tested for Reynolds number dependence and was found to be independent for the boundary conditions tested in the Phd study. Also the new airfoil R-opt, which was developed for the rotor with the exchangeable tips, was optimized to operate stable at low Reynolds numbers. Nevertheless, it should be kept in mind that the wind tunnel experiments are affected by scaling effects and do not represent the full-scale exactly.

2.4 Measurement technique

In the experiments carried out in this study, different measurement techniques were used to study turbine power, forces acting on the turbine and various wake properties. Most of the measurement devices provided analog signals, which were transformed to digital signals and conditioned using DAQ (data acquisition) system devices from National Instruments. Before transforming the analog signals to digital signals, they were amplified by in-house amplifiers in order to be able to use the whole measurement range from -10 V to +10 V of the 16-bit DAQ systems and thus limit discretization errors. The digital voltage signals were analyzed and recorded using a computer with a LabView routine. The transformation of the voltage data to the desired variables and the evaluation of this properties was conducted with MATLAB.

2.4.1 Power measurement technique

The hub of the model wind turbines T1 and T2 is equipped with measurement technique to determine the rotor power. In Figure 2.13, the hub of T2 and a sketch of its cross-section are pictured. It can be seen that the hub is equipped with a torque transducer to measure the shaft torque M and an optical RPM sensor to determine the rotational speed of the rotor. With these two parameters the rotor power can be calculated according to $P = M \cdot \omega$.

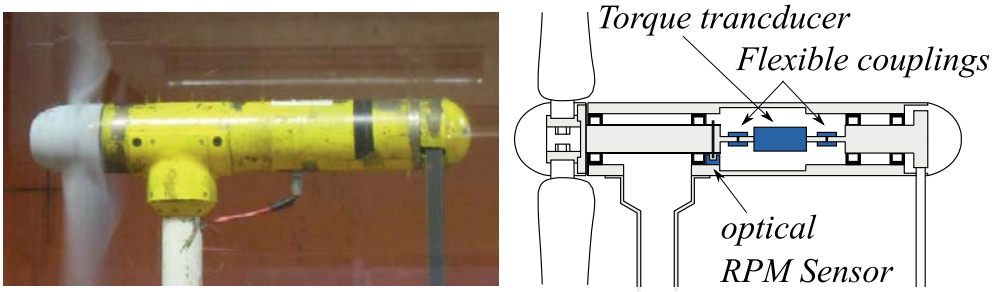

Figure 2.13: Picture of the turbine hub of T2 and a sketch of its cross-section showing the setting with the installed measurement technique (blue) inside the hub.

The Hottinger 2 N torque transducer is located to the rotor as close as possible. With this setting only the roller bearings are located between the rotor and the transducer and thus the shaft friction losses are limited. Furthermore, flexible couplings before and after the transducer secure this highly sensitive measuring device from load peaks. The transducer was calibrated prior to all the measurements by applying a range of reference weights at the blade tips (see Figure 2.14). The calibration process resulted in a linear relation between the rotor torque and the voltage signal. Furthermore, the calibration factor was observed to be stable throughout all experiments and only varied insignificantly.

Figure 2.14: Calibration process of torque transducer.

The optical RPM sensor provides a signal amplitude at a fixed rotor position for every revolution of the turbine rotor. With the time span between the signals the rotational velocity of the rotor can be calculated. Furthermore, the RPM signal was synchronized with the other measured signals to determine the rotor position were the other measurands were obtained. Due to this arrangement, the data could be analyzed in relation to the rotor position to get phase-locked information. Such phase-locked data was generated and investigated in the wake experiments of the winglet rotor for *Paper III*.

2.4.2 Force measurement technique

For the force measurements the model turbines were installed on a aerodynamic balance, which is located under the wind tunnel floor. With the six-component force balance from the Carl Schenck AG, it is possible to measure all force components acting on the model turbines and calculate the aerodynamic moments with the accompanying lever arms. For the experiments, only the three horizontal load cells were used and in most experiments, only the component in flow direction was considered to obtain the thrust force acting on the turbine and rotor assembly. All three components were recorded in the experiments for *Paper VI* and *Paper VII* in which - in addition to the thrust force - the yaw moments were analyzed. In some studies the solely rotor thrust was of interest. Therefore, the thrust force acting on the turbine rig without the rotor was measured separately and subtracted from the total thrust. All load cells were calibrated separately prior to every measurement by applying defined reference weights on the load cells. Similar to the torque transducer, a linear relation between the force and voltage was obtain in the measurement range. Furthermore, the aerodynamic balance served as a rotating table for the turbine models. This enabled a control of the yaw angle from outside the wind tunnel.

2.4.3 Wake measurement technique

For measuring the wake flow mainly two measurement techniques were used. In the experiments for *Paper I*, *Paper II*, *Paper V*, *Paper VI* and *Paper VII*, the wake properties were measured with a LDV (Laser-Doppler velocimetry) system. Only in *Paper III*, where phase-locked data was acquired, a Cobra probe was used for the velocity measurements. This technique was chosen because it could be synchronized with the other measurement devices and the data could be obtained at a defined rotor position with a fixed sampling frequency. The measurement devices were mounted on a traverse system in the wind tunnel that was controlled from outside with a LabView routine. With this setting, the wake measurement devices could be traversed in the wake flow.

Laser Doppler velocimetry

The most applied velocity measurement technique in the PhD study was LDV. All the measurements were conducted using a 2-component Dantec FiberFlow LDV system, which is shown in Figure 2.15. With the LDV technique, it is possible to measure flow velocities with a high temporal resolution and thus get not only time-averaged mean velocities, but also time-independed flow information.

LDV is an optical measurement technique, which is non-intrusive and does not need calibration. Furthermore, the velocities do not need to be transferred from voltages but are provided directly and in real time. Therefore, the voltage signals are processed by so called burst spectrum analyzer (BSA) and analyzed by the accompanying BSA flow software. The laser beam is generated by a air-cooled Argon-ion laser with up to 300 mW per wavelength. In the transmitter, the laser beam is split into two beams by a bragg cell and each of these beams is separated into the two colors green ($\lambda_{\mathrm{LDV}} = 514.5$ nm) and blue ($\lambda_{\mathrm{LDV}} = 488$ nm). With the four manipulators, the lasers are adjusted so that the maximum amount of light is linked to the fibers directing the beams into the probe, from where they are transmitted and the back scattered light is received.

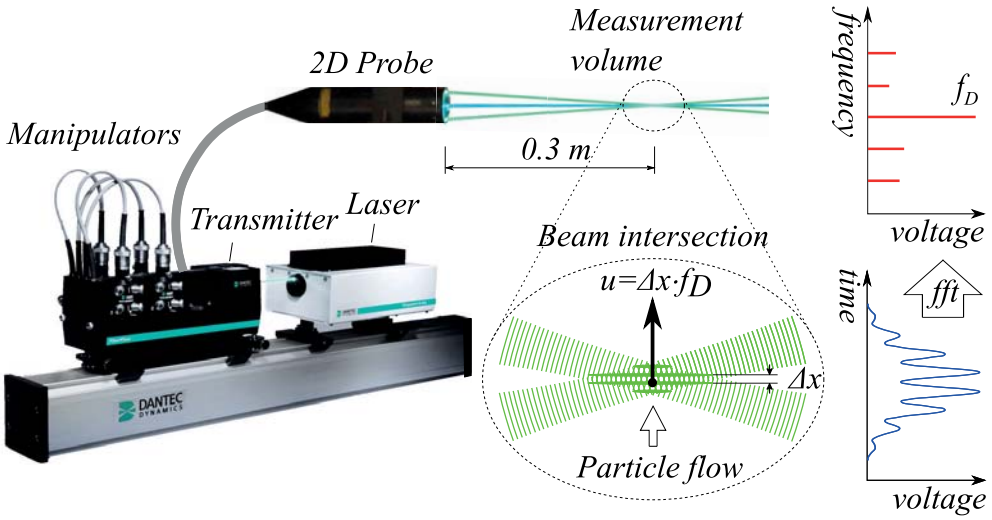

Figure 2.15: Picture of the turbine hub and sketch of the setting with the installed measurement technique (blue) insight the hub.

The measurement principle of the LDV system is briefly sketched in Figure 2.15. It can be seen that with the LDV technique, the velocity of the airflow is not measured directly, but the velocity of particles moving in the flow. The measurement volume is formed by two laser beams of similar intensity, which are transmitted from the LDV probe, where they are focused to intersect and form a fringe pattern with the known interval Δx. When a particle is passing through the fringe pattern it scatters light back to a receiver in the probe. This back scattered light contains a frequency shift entailed by the Doppler frequency f_D of the moving particle, which is proportional to the velocity of the particle passing through the fringe pattern. This optical signal is converted to a voltage signal, which is filtered and amplified and then transformed to the frequency domain by a Fast Fourier Transformation (FFT) in order to determine

f_D. As the distance traveled by the particle is given by Δx and the time of this travel is contained in f_D the velocity of the particle can be calculated by $u = \Delta x \cdot f_D$.

The LDV probe was installed on the wind tunnel traverse and adjusted by leveling the reflections on the wind tunnel wall or floor and aligning them with the probe. The LDV system was adjusted to only take samples into account that were recorded by the lasers in both measurement directions. In the experiments $5.0{\cdot}10^5$ samples were recorded for every measurement point. The acquisition data rate was adjusted by controlling the particles in the flow. Throughout the measurements the acquisition data rate was between 1 500 Hz and 2 500 Hz what resulted in a measurement time between 20 s and 35 s. The particles with a size between 0.5 μm and 2.0 μm were created with a thermal smoke generator that was located at the end of the test section. In that way the particles traveled through the whole wind tunnel where they distributed evenly before entering the test section.

Cobra probe

For the investigation of the wake flow of the rotor equipped with winglets in *Paper III* a Series 100 Cobra probe from TFI (TurbulentFlow Instrumentation) was used. This measurement technique was selected, because with this device it is possible to synchronize the turbine rotation and the velocity measurements and allocate measurants to an exact turbine position to obtain phase-locked wake data.

The Cobra probe, which is shown in Figure 2.16, is a 4-hole Pitot tube in which the pressure transducers are located directly in the probe body. The short tubing between the pressure tabs together with a linearisation process, correcting for pressure fluctuations in the tubing, enables the Cobra probe to measure not only time-averaged mean velocities but also time-varying turbulent velocity components (Hooper and Musgrove, 1997).

The Cobra probe does not require extensive calibration, as the probe head has a defined geometry (see Figure 2.16) and the calibration process is performed by the manufacturer who provides calibration tables for the individual probes. The pressure regime at the probe head, which is determined by the four pressure values measured at the tabs, can be assigned to the three velocity components u, v and w as well as the static pressure at the tip of the device by applying the calibration tables. Detailed information of the calibration process and the transformation from the pressures to the velocities is provided by Shepherd (1981)

In the PhD study, the four voltage signals provided by the Cobra probe were evaluated by a MATLAB routine with implemented interfaces of the manufacturer TFI providing the calibration tables. The analysis resulted in the time-varying velocities

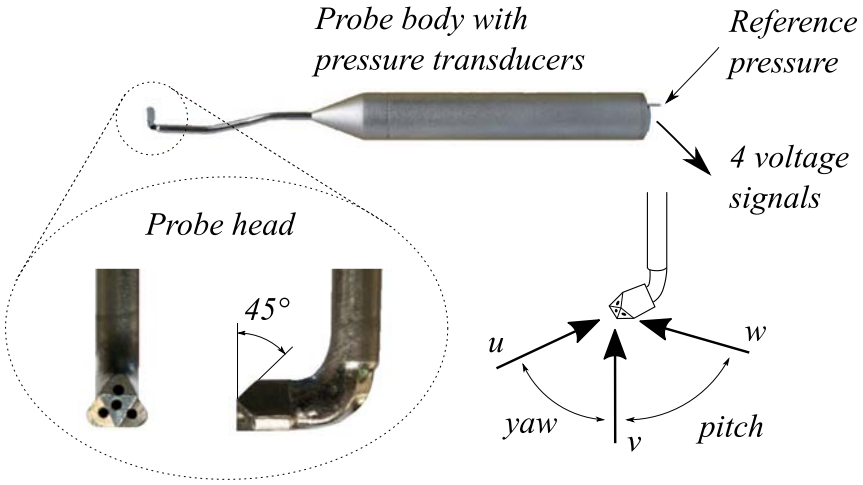

Figure 2.16: Series 100 Cobra probe, with detailed probe head geometry and the flow axis system.

of the three components, which were used to calculate the other flow properties like the time-averaged velocities, the flow angles and the turbulent kinetic energy (TKI). In order to obtain accurate results, the flow angles must be within 45°. Therefore, all measurements in which one of the flow angles was bigger than 45° were excluded from the analysis.

The Series 100 Cobra probes used for the study have a frequency response of 600 Hz. In order to obtain phase-locked data one rotor revolution was divided in 120 section, each of 3°. With a rotational speed of 1 280 RPM this resulted in a required frequency response of at least 2 560 Hz in order to get information for every rotor position per revolution. In order to sample the data with a frequency response of 2 560 Hz, the usable frequency range was extended by changing the transfer function cut-off amplitude for the linearization process. With this measure the response of the probe was extended to over 3 000 Hz. Nevertheless, the disadvantage of this method is, that signals with frequencies >1 000 Hz need to be amplified, because such signals appear too weak at the transducers. Consequently, also noise is amplified, which increases the measurement error. In order to avoid aliasing, the data acquisition rate was 10 240 Hz resulting in an over-sampling ratio of 4.

For the experiments, two Cobra probes were used simultaneously, to reduce the time for the measurements. Therefore they were installed in a support, carrying them with a defined distance of separation. One of the biggest challenges is to install the probes straight in the wind tunnel. In order to achieve this, the velocities were measured with the LDV probe and the Cobra probe at the same position. The direction of the Cobra probes was adjusted until the measurement devices measured the same velocity components, resulting in identical flow angles. The procedure is pictured in Figure 2.17.

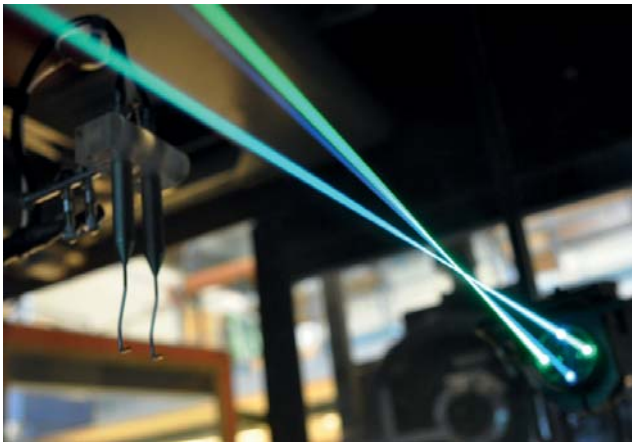

Figure 2.17: Simultaneous measurements with LDV and Cobra probe for adjustment of Cobra probe head.

2.5 Measurement uncertainty

Experimental measurements are not perfect. They are always afflicted with some deviation between the true value and the measured value. This error has various sources and can typically be divided into the two categories systematic and random errors, see Figure 2.18.

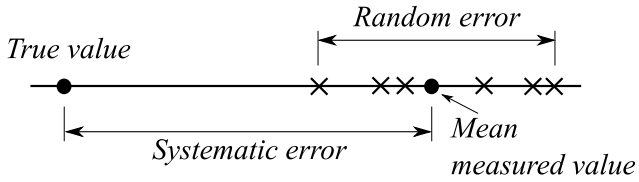

Figure 2.18: Explanation of systematic and random error.

Systematic errors can be described as repeatable and consistent, meaning that they are not changing during the experiment. Random errors are caused by unpredictable changes in the experiment, which are not known and thus can not be repeated. Usually, the real error of a measurement is unknown and cannot be determined. A method to evaluate how accurate an experiment was and to quantify the error, is to calculate the uncertainty of a measurement. The measurement uncertainty is an estimated range, in which the error will be arranged based on a confidence interval.

Measurements of all individual parameters are afflicted with uncertainties that propagate to a total uncertainty of the final result. For example, the measured quantities temperature *Temp*, ambient pressure p_{amb}, inlet velocity U_∞, rotational speed of the rotor ω and shaft torque M are needed to calculate C_P (Equation (2.4)) and each parameter features an inaccuracy that will affect the total uncertainty of the final result for C_P.

To obtain the total uncertainties of the investigated parameters in this work the procedure described by Wheeler and Ganji (2010) was applied. Therefore, the measurement process was outlined in the beginning and the relation between the final result and all depended parameters was defined. For all the parameters possible error sources containing errors due to calibration, data acquisition, data reduction methods and other sources were listed. For each individual source, the errors were determined. The systematic errors were estimated based on manufacturers specifications or from previous studies and observations. For the random errors the standard deviation of the measured parameters was calculated. To get the standard deviation of the turbulence properties the standard deviation was calculated based on the technique described in (Benedict and Gould, 1996). With all the individual error terms the total systematic uncertainty was calculated using a root of the sum of the squares:

$$B_R = \left\{ \sum_{i=1}^{n} \left(B_i \frac{\partial R}{\partial x_i} \right)^2 \right\}^{1/2}, \tag{2.24}$$

where B_i is the systematic error of the individual parameter and and $\frac{\partial R}{\partial x_i}$ is the derivative of the overall parameter with respect to the individual parameter. The random uncertainty for every measurement point is calculated with:

$$P_R = \pm t \frac{\sigma}{\sqrt{n}}, \tag{2.25}$$

where t is the value of the Student's t, σ is the standard deviation and n is the number of measurements. The resulting individual error terms are combined to the total uncertainty by the root of the sum of the squares, similar to that of the systematic uncertainty. The total uncertainty is calculated by a combination of both uncertainties:

$$\varpi_R = \sqrt{B_R^2 + P_R^2}. \tag{2.26}$$

In this study, all uncertainties were estimated based on an 95%-confidence level. The analysis of the uncertainties for the different investigated quantities suggested that systematic errors had the largest contribution to the total uncertainty. Nevertheless, also random uncertainties were distinguished, which could be seen in higher levels of uncertainty in turbulent flows.

Typical uncertainties for mean velocities measured with the LDV system were around 1% whereas the turbulence from these measurements featured slightly higher uncertainties around 2%. The measurements with the Cobra probe featured higher uncertainties, which were typically up to 5% for the velocity and 8% for the turbulence.

Typical uncertainties of the power coefficient C_P were found to be approximately 3% around the optimum tip speed ratio of the rotor. Outside this region the results were affected by less inaccuracy. For the thrust coefficient C_T, the uncertainty was observed to rise with increasing tip speed ratios reaching uncertainties of up to around 2%.

Chapter 3

Summary of main results

This chapter summarizes the main results of the PhD study and the main findings of the papers will be presented. The contribution to the field of wind farm optimization will be discussed in beginning. Within this field, the study comparing the wake of 2- and 3-balded wind turbine rotors will be presented. Afterwards, the main findings of the project analyzing counter rotating wind turbine rotors will be shown. The third rotor modification concept that will be presented examines the effect of winglets on wind turbine blades, in which the design of the winglets and their influence on the wake development will be discussed. The wind farm optimization will be finalized by presenting the results of the wind turbine wakes in yaw project, where the potential of intentional yaw misalignment for wind farm control optimization will be shown. The summary of the main results will be completed by presenting the findings of the Blind test comparison, where reference data was provided for CFD validation.

3.1 Wind farm optimization

For the main part of the PhD thesis rotor-wake interactions were investigated to evaluate different methods, which were deemed to have the potential to optimize the power output of wind farms. Firstly the approach of modifying the rotor design to limit wake effects was studied. Within this technique the effect of the blade number on the wake development was studied by comparing wake properties of 2- and 3-bladed model wind turbines in *Paper I*. Furthermore, the influence of the rotational direction of the wind turbine rotors in a wind farm was investigated in *Paper II* by comparing the performance of an aligned turbine array with co- and counter-rotating rotors. The third rotor design modification that was studied, was a rotor equipped with winglets. For this study, a new rotor was designed and winglets for this rotor were optimized

before comparing the performance of the rotor with and without winglets in *Paper IV*. The winglet rotor's effect on the wake was investigated in *Paper III*, where wakes of rotors with and without winglets were compared. The second approach for wind farm optimization that was considered in the project was improving the turbine control by intentional yaw misalignment. In order to apply yaw control it is important to know how the wake flow of a yawed turbine. To provide more information about the wake structure *Paper V* investigates the influence of different inflow conditions on the wake shape and development. The power and loads of a turbine array in various yaw configurations are discussed in *Paper VI*.

3.1.1 Comparison of 2- and 3-bladed rotors

The costs of a wind turbine can be reduced if 2-bladed rotors instead of common 3-bladed rotors are used. However, using 2-bladed rotors is accompanied by several disadvantages like higher noise emissions, distracting visual effects and unfavorable dynamic behavior (Hau, 2013). Those disadvantages are deemed to be the reason why the research effort on the wake development of 2-bladed rotors was limited and only few studies on this topic exist.

In an experimental study, Newman et al. (2015) investigated wake effects in scaled down wind farms consisting of 12 small model wind turbines with 2- and 3-bladed rotors with similar C_P. They found large differences of mean streamwise velocities in the near wake of the array, where the wake of the 2-bladed rotors showed higher mean velocities. However, in the far wake the differences between the two rotor concepts for the mean velocities where only insignificant. Furthermore, the streamwise Reynolds stresses were observed to be higher in the wake of the 3-bladed turbines leading to higher fatigue loading on the downstream turbines.

Analytical wake models suggest that the blade number does not have an influence on the velocity in the wake as they do not take the blade number into account (Polster et al., 2017). The main parameter determining the wake flow in the models is the thrust coefficient C_T, which was similar for the tested rotors in the study. However, there might be differences in the wake flow as already suggested in the study by Newman et al. (2015). Especially the turbulence intensity is expected to be different in the wake behind the 2- and 3-bladed rotors, as the stronger tip vortices of the rotors with only two blades are deemed to increase the turbulence levels behind the rotor edge. Therefore, the wake of 2- and 3- bladed turbines were compared in *Paper I*.

The differences of the wake properties between the 2- and 3-blade rotors from the line wakes of *Paper I* are summarized in Table 3.1. The available power in the wake ($P_{ava} = 0.5\rho A_R U_\infty^3$). was calculated in order to compare the velocities in the wake. It

can be seen that the differences in the available power and thus the mean streamwise velocities are only minor. This is confirmed by similar wake recovery rates for all three rotor concepts. Furthermore, full wake scans of the mean streamwise velocity at $5D$ reveal no major differences and thus verify these observations. Comparing the turbulence in the wake there also is no indication of big differences between the wakes of the three rotors. Nevertheless, it can be seen that the turbulence levels in the wake behind the 2-bladed rotors are higher than those of the 3-bladed rotor at all investigated distances, whereas the differences become smaller with increasing distance. The major discrepancies in TI occur mainly behind the tip region and are caused by the stronger tip vortices of the 2-bladed rotors, which decay with increasing distance.

Table 3.1: Summary of differences in available power (P_{ava}) and turbulence intensity (TI) in the wake behind the 3-bladed rotor (Rotor1), the 2-bladed rotor with the same aspect ratio (Rotor2) and the 2-bladed rotor with the same solidity (Rotor3).

		Rotor1 - Rotor2	Rotor1 - Rotor3
3D	P_{ava}	1,3%	0.2%
	TI	-0.5%	-1.9%
5D	P_{ava}	1,0%	-3.0%
	TI	-0.5%	-1.2%
7D	P_{ava}	1,1%	-3.2%
	TI	-0.2%	-0.2%

It can be concluded from the study that the wakes of 2- and 3-bladed rotors are similar. The differences in mean streamwise velocity are minor and the turbulence intensity is only varying for the blade number at small distances and is equalized at typical separation distances of wind turbines. As a result, using turbines with 2-bladed instead of 3-bladed rotors does not improve the power output of a wind farm. Nevertheless, 2-bladed rotors do not have a negative influence on wake interactions and can therefore be used in wind farms to decrease installation costs, without affecting the overall power.

A weakness of the study is displayed by the circumstance, that the C_P's of the 2- and 3-bladed rotors do not match at the tip speed ratios where the turbines were operated. The 2.7% higher C_P of the 3-bladed rotor makes it difficult to draw reliable conclusions about the overall performance of a wind farm. To solve this problem, new 2-bladed rotors with higher C_P's that exactly match that of the 3-bladed rotor need to be designed and the wake of these rotors need to be compared to the 3-bladed rotor. Furthermore, an experiment investigating the overall performance of an aligned

2-turbine array would be necessary to draw a reliable conclusion about the different energy content in the wake of 2- and 3-bladed turbines.

3.1.2 Counter rotating wind turbine rotors

From Figure 3.1 can be seen, that the wake behind a clockwise rotating wind turbine is rotating counter-clockwise and thus opposite to the turbine rotor. Consequently, the inflow of a downstream turbine operating in the wake of an upstream turbine contains a tangential velocity component in opposite direction to the rotor rotation. This additional velocity component is changing the velocities at the rotor plane, which could affect the performance of the rotor. It might have a positive effect on the rotor performance if this additional velocity component is orientated in opposite direction and thus in the direction of the rotor rotation. Consequently, it might be beneficial to use a mirrored rotor design for the upstream turbine to get an array with counter rotating turbines. However, only little attention has been paid to this topic and only few studies, which investigate the effect of alternating rotational direction in a wind farm, exist.

An experimental study on this topic was conducted by Yuan et al. (2013, 2014), who investigated an aligned tandem turbine array with co- and counter rotating rotors. They showed that the counter-rotating array was more efficient as the co-rotating array in extracting power. The performance increase was found to be up to 20% at a separation distance of $0.7D$, but decreased with increasing distance and was found to be negligible from $6.5D$ on. Nevertheless, the study showed the potential of counter-rotating turbines for the optimization of wind farms. Therefore, the effect of the rotational direction on the wake of a wind turbine rotor was investigated in *Paper II*.

In the study for *Paper II* the wake was analyzed with special focus on the tangential velocity component. Furthermore, the performance of a two-turbine array with co- and counter-rotating rotors was compared. In addition to the experiments, a BEM code was used to study the effect of the additional tangential velocity component on the blade loads and the performance of the aligned turbine array.

The BEM analysis of the flow around the blade showed that the additional tangential component in the inflow changes the flow angle. As a result, the angle of attack on the downstream rotor decreased in the co-rotating array, whereas it increased in the counter-rotating array. The performance comparison of the tandem turbine arrays showed no big differences between the co- and counter-rotating array. However, the counter-rotating array had a slightly better performance at all investigated turbine separation distances. At $2.00D$ the combined C_P was 1.2% higher, at $3.50D$ and

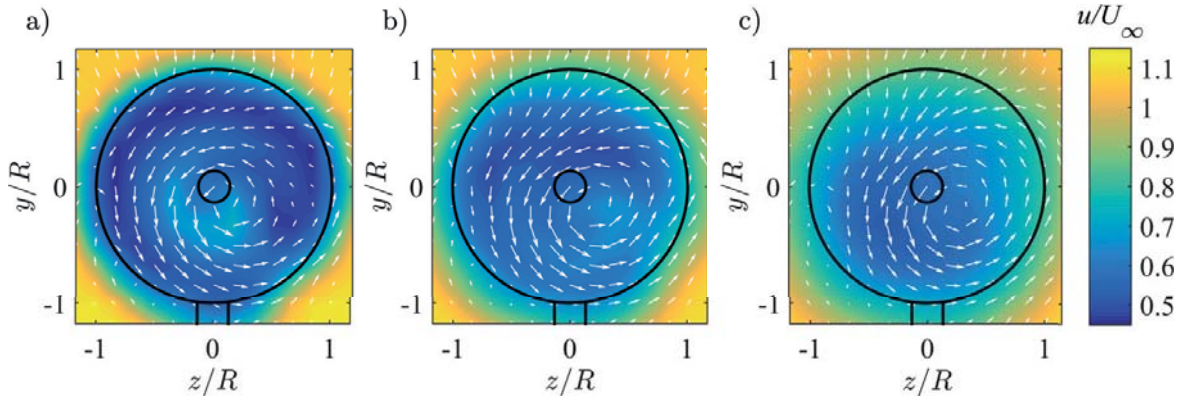

Figure 3.1: Contour plots of normalized streamwise mean velocity, with arrows representing the resultant of the vertical and horizontal velocity component, in the wake (a) $2.00D$, (b) $3.50D$ and (c) $5.15D$ behind the clock-wise rotating 3-bladed rotor mounted on turbine T2, the black lines represent the turbine rotor, nacelle and tower, locking in flow direction.

$5.15D$ the difference was 2.0% and 0.6%, respectively. This was confirmed by the BEM calculations, which were generally between 5% and 7% lower as the experimental results, but showed the same trends.

However, as the performance improvement stems from a increased flow angle, the same effect could be generated by changing the pitch angle of the blade. This observation is confirmed by Bartl and Sætran (2016), who investigated the C_P of the same rotor for a variation of pitch angles and found a higher C_P if the twist angle was greater than the one applied in the study for the counter rotating wind turbine rotors.

From this observation and the small differences in C_P of the co- and counter-rotating turbine array can be concluded, that the optimization potential of alternating rotational directions in a wind farm is insignificant.

3.1.3 Winglet rotor

Most modern airplanes are equipped with winglets to improve their efficiency (Figure 3.2). The additional winglets reduce the fuel consumption by around 4-5% for transport airplanes (Freitag and Schulze, 2009). Winglets improve the performance of a wing by reducing the induced drag, which is generated at the blade tip where the pressure difference between the pressure and suction side of the blade is equalized and a vortex is formed. The resulting span wise flow from the pressure to the suction side influences the lift and drag at the tip and further inwards and the lift of the wing is reduced (see Figure 3.3). A winglet reduces this span wise flow and consequently helps to limit the reduction of lift.

Figure 3.2: Winglet on the wing tip of a transport airplane.

From the performance enhancement achieved in aviation it can be concluded, that winglets might also have the potential to improve the performance of a wind turbine. Consequently, several studies investigating the effect of winglets on wind turbine rotors have been conducted.

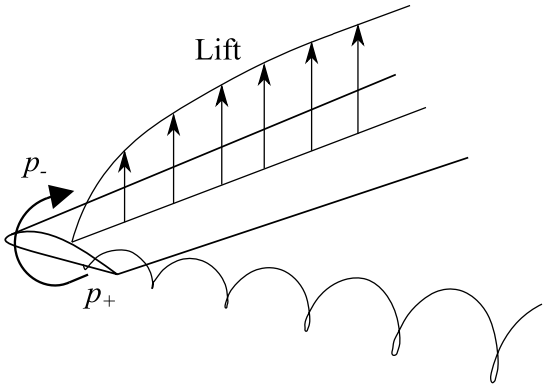

Figure 3.3: Pressure equalization at the blade tip and the resulting tip vortex and lift distribution.

Johansen and Sørensen (2006) designed six winglet shapes, and analyzed them with the EllipSys3D solver. They showed that winglets can improve the performance, but also worsen it if not properly designed. Their best design increased C_P by around 1.0%, which was accompanied by an increase in C_T of 1.6%. In a further study, they used the same CFD solver to perform a parameter study changing the height, curvature radius, sweep angle and twist angle of a winglet (Johansen and Sørensen, 2007). They designed and investigated 10 winglet concepts and their results show that the winglet height has the biggest influence on the C_P and C_T. Whereupon a winglet with a height of 4% of the rotor radius had the highest C_P and C_T increase of 2.6% and 3.6%, respectively. Gaunaa and Johansen (2007) also used the EllipSys3D solver to investigate winglets, which they designed with a self-developed free wake lifting line code. They showed that downwind winglets are more effective than upwind winglets. Maniaci and Maughmer (2012) designed downwind winglets with the height of 8%

rotor radius for a model-scale wind turbine (D = 3.3 m). Results of wind tunnel experiments with this rotor showed an increase in C_P of 9% and confirmed the large influence of winglet height on the performance. The same rotor was used by (Gertz et al., 2012, 2014) who tested different winglet designs and found performance increases between 5% and 8%. The wake formed behind a rotor with downwind winglets was experimentally studied by (Tobin et al., 2015). They found an increased velocity deficit in the wake of the winglet rotor. However, they predicted that this deficit could be evened by the higher C_P of the winglet rotor and increase the total C_P of a turbine array. Furthermore, they found similar tip vortex strength for the winglet and baseline rotor. In his PhD thesis Ostovan (2017) investigated the performance of an aligned turbine array operating with and without down-facing winglets and found an increase in overall efficiency if winglets were installed on the upstream turbine. Furthermore, he measured the tip vortices in the very near wake and estimated an induced drag reduction of around 15%.

All these studies show that additional winglets on wind turbine rotors have the potential to increase the performance of a single turbine and turbine array. To further investigate this promising technique, in *Paper IV* a new rotor was designed and winglets for this rotor were optimized for an increased C_P. Furthermore, the growth in C_T was limited in the optimization to reduce wake effects. In *Paper III* the wake behind this new rotor was investigated experimentally and compared to the baseline rotor without winglets.

During the optimization process the six design parameters span, sweep, angle of attack, radius, root chord and tip chord were varied and over 100 different designs were investigated numerically. The optimal winglet for the rotor in the design framework was found to have a span of 10.8% of the rotor radius. According to the CFD simulations the winglet increased the rotor power by 7.8% and the thrust by 6.3%. This was confirmed by the experiments, which showed an increase of C_P and C_T of 8.9% and 7.4%, respectively. The same increase in C_P was achieved by increasing the blade radius by 3.6%. Analyzing the rotor blade flow showed that the winglet improves the rotor performance mainly by increasing the lift in the tip region of the blade. In this region the induced drag is reduced because the pressure difference is shifted from the blade tip to the winglet.

The experimental wake study showed that up to $4.0D$ downstream the differences in mean streamwise velocity between the winglet and baseline rotor are small, suggesting a minor effect of blade tip extensions on the combined efficiency of a wind farm. The investigation of total kinetic energy, revealed slightly higher initial energy peaks in the tip region, when winglets were attached to the rotor tips. Starting from a dwonstream distance of approximately $2.0D$, the shear layer behind the tip region was observed to be

significantly broader for the wingletted configuration. An analysis of the out-of-plane vorticity showed that the tip vortices of the wingletet rotor were breaking around $1.0D$ earlier as those of the rotor without winglets. Furthermore, higher absolute vorticity was found when winglets where mounted on the rotor.

The winglet study showed that it is possible to design winglets, which increase the wind turbine performance with a moderate growth of rotor thrust. Furthermore, it confirmed the findings from literature that winglets can help to improve not only the performance of a single turbine but also those of a turbine array consisting of multiple turbines.

However, the investigation of the blade extension showed, that a by 3.6% increased rotor radius has the same effect on the C_P as the winglet with a span of 10.8% of the radius. In conclusion, winglets make most sense if the rotor diameter is limited, which can be the case for offshore applications, where the costs of the tower can be reduced if its height is limited. Nevertheless, winglets are deemed to be a good possibility to optimize a wind farm by a modified rotor design.

3.1.4 Yaw wake control

Usually a wind turbine is aligned with the flow to extract most energy possible from the wind. However, if the rotor is not perpendicular to the wind direction, the velocity experienced by the rotor decreases with the cosine of the yaw angle γ (see Figure 3.4). As a result, the power of the rotor reduces. Moreover, the thrust force of the rotor T contains a streamwise and lateral force component. The resulting lateral force component introduced by the yawed rotor F_z deflects the wake sideways. As a result, the wake trajectory can be controlled by intentionally yawing the rotor. Even though such a yaw misalignment would decrease the turbine performance. The overall efficiency of a wind farm could be increased if the wake is directed away from a downstream turbine leaving more energy in its inflow. Such wake redirection is considered to be a promising technique to improve wind farm control (Gebraad et al., 2016).

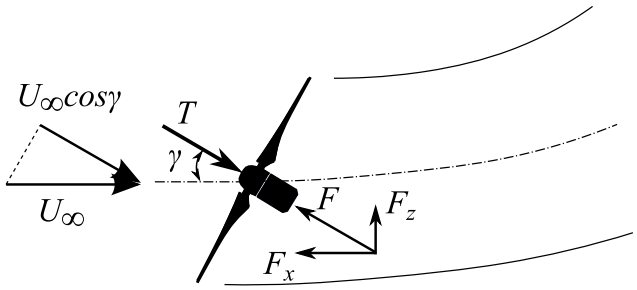

Figure 3.4: Sketch of forces induced by a yawed wind turbine and the resulting lateral wake deflection.

Among wake redirection techniques, yaw misalignment is deemed to have the largest potential for increasing the farm efficiency (Fleming et al., 2014). Therefore, several studies investigating the wake development behind a yawed turbine have been conducted. In an experimental study Medici and Alfredsson (2006) analyzed the wake behind a small yawed model turbine of $D = 0.18$ m. They investigated a yaw range from $\gamma = 0° - 20°$ and found a distinct deflection of the wake, caused by a clear cross-stream flow component. Krogstad and Adaramola (2012) used a larger turbine of $D = 0.9$ m, on which they showed that the power output decreased proportional to $cos^3\gamma$. They furthermore investigated the near wake and found a dependency of the wake deflection and structure on the turbine's tip speed ratio. Bastankhah and Porté-Agel (2016) performed an extensive experimental particle image velocimetry (PIV) study on the wake of a yawed model wind turbine of $D = 0.15$ m. Their results confirm the wake's dependency on factors like wake rotation and tip speed ratio. A combined experimental and numerical study was performed by Howland et al. (2016) who investigated the wake behind a small drag disc of $D = 0.03$ m. They show that the yawed non-rotating disc has a realistic wake deflection. In their analysis of the wake shape, they found an asymmetric so-called curled wake shape, which is created by a counter-rotating vortex pair. In another experimental study, Schottler et al. (2016b) investigated the performance of an aligned turbine array and showed an asymmetric power output depending on the upstream turbines yaw angle. This asymmetric behavior was also observed by Fleming et al. (2014), who performed a numerical study based on Large-eddy simulations (LES) and found a slightly different wake deflection depending on the yaw direction. Gebraad et al. (2016) performed another CFD study using the SOWFA solver and confirmed the large potential of intentional yaw misalignment for wind farm control optimization. The influence of atmospheric stability on the wake of yawed turbines was numerically investigated by Vollmer et al. (2016). They show that the wake shape and skew is highly depended on the atmospheric stability. In a recent CFD LES study Wang et al. (2017) showed the importance of including tower and nacelle in the simulations. Moreover, also full-scale experiments investigating the effect of yaw were carried out. Trujillo et al. (2016) used LiDAR to track the near wake behind a 5 MW offshore wind turbine for a yaw range from γ = -10.5° – 10.5°. In another full-scale study Fleming et al. (2016a) applied a yaw wake-steering open-loop controller to a wind turbine array. Their study showed that the power output of two turbines was improved by yaw based wake steering. Jiménez et al. (2010) used the experimental results from Medici and Alfredsson (2006) to verify LES simulations around a yawed actuator disc. From the numerical results they derived an analytical momentum conservation based wake model for predictions of the velocity deficit and wake trajectory of a yawed wind turbine. Bastankhah and Porté-Agel (2016) used

the results of their extensive experimental and numerical studies to develop another analytical model for the far wake of a yawed wind turbine, which also accounts for inflow turbulence.

Despite the large potential of yaw control for wind farm optimization found in the literature, the existing studies point out the need for detailed wake measurements of yawed turbines. In order to provide such data a collaborative project on wind turbine wakes in yaw was initialized between NBMU, NTNU and ForWind in Oldenburg. The wakes behind two yawed wind turbine models of different design, were investigated extensively under various inflow conditions in the NTNU wind tunnel. The experimental results of the project are the basis of *Paper V*, which investigates the influence of inflow turbulence and shear on the wake structure and *Paper VII*, which compared the experimental results to numerical predictions. Furthermore, the measurements were used for the additional *Papers X* and *XI*, where the wake of the two model turbines was compared. The detailed data sets from the wind turbine wakes in yaw project are published by Schottler, Bartl, and Mühle (2018). Additional to the wake experiments, a two-turbine array was investigated at various differing yaw and lateral offset configurations. With the results of this experiment the potential of power and load optimization of yawed wind turbines was discussed in *Paper VI*. Furthermore, the far wake of a smaller yawed turbine rotor of $D = 0.45$ m was experimentally investigated and analyzed in the additional *Paper XIV*.

The analysis in *Paper V* revealed minor asymmetries in the wake between positively and negatively yawed rotors, which stem from tower wake interactions. The asymmetries were found to be larger for the lower inflow turbulence. The inflow turbulence also influenced the shape of the wake, which had a clear kidney shape for all inflow conditions, whereas it was more distinct at larger downstream distances. Moreover, the wake deflection was observed to be slightly different for the two investigated levels of inflow turbulence. Furthermore, the moderate shear in the inflow was found to have little influence on the wake properties. The study shows, that the turbulent kinetic energy in the wake is deflected to the same degree as the mean streamwise velocity profiles, while its expansion is slightly wider. Furthermore, it was shown that the levels of peak turbulence decreased similarly to the rotor thrust if a yaw angle is applied.

The power and load optimization study in *Paper VI* showed that the combined power of a two-turbine array could be increased by intentional yaw misalignment of the upstream turbine. The largest improvements for a yaw angle of $\gamma = 30°$were found at a separation distance of $6D$. For this arrangement, the total performance increased up to 11% for the low-turbulence and 8% for the high turbulence inflow. This discrepancy confirms the strong influence of inflow turbulence on power gains if yaw control is applied. Furthermore, the power gains were found to be asymmetric due to

the different wake shape and deflection for positive and negative yaw angles. Although, the total power could be increased by yawing the upstream turbine, the yaw moments for the upstream and downstream turbine both increased. By applying a lateral offset of $0.5D$ most of the wake could be steered away from the downstream turbine, which resulted in an increased total power and reduced yaw moments. Furthermore, it was demonstrated that yawing the downstream turbine opposite to the upstream turbine mitigated the yaw moments and increased the total power.

The wind turbine wakes in yaw project resulted in more publications, which are not included in the thesis. The main findings of these articles are described below. In the additional *Paper X* the available power method, which was used for the quantification of the wake deflection in wind turbine wakes in yaw study is established. Two-point statistics of the wake properties are investigated in the additional *Paper XI*. The results reveal a ring of strongly intermittent flow around the mean velocity deficit, in the wake of the yawed turbine, resulting in a wider wake expansion as if only considering the mean velocity. The findings show the importance of considering non-Gaussian distributions of velocity increments for wind farm control optimization. In the additional *Paper XIV* the focus is on the far wake trajectory. The results of this paper show that the wake deflection has an asymptotic behavior and the skew angle is almost zero in the far wake.

The study on wind turbine wakes in yaw confirmed that intentional yaw misalignment is an effective method to laterally deflect the wake and thus has large potential for the power optimization of wind farms. However, the rotor blades of a yawed rotor experience unsteady flow conditions in the course of one rotation which resulted in increased loads on the yawed turbine. The same applies for turbines operating in a partial wake of a yawed turbine. Consequently, loads have to be taken into account when optimizing the wind farm control. A possibility for load reduction is yaw control of the downstream turbine. By yawing the downstream turbine opposite to the upstream turbine not only the loads can be reduced, but also the power can be increased.

3.2 Reference data for CFD validation

CFD simulations are a good technique to study rotor-wake interactions of wind turbines. However, as mentioned in Section 1.1.5, CFD codes and the applied turbulence models need to be validated with actual measurement data in order to determine their accuracy. To help with the validation and the further development of CFD codes, selected results of the experiments with the yawed turbines were compared to computational results in *Paper VII*. Furthermore, the data sets were published so that they can be used as reference data for the validation of new CFD simulations.

3.2.1 Blind test comparison

In the Blind test series, which was initiated by NTNU in 2011, experimental data of turbine performance and wake flow is compared to numerical predictions. In each Blind test, specific test cases for turbine arrangement and operation in the wind tunnel are defined and the turbine performance and wake properties are measured according to the description of these test cases. All the information, which is needed to reconstruct the test cases in a CFD domain, including boundary conditions as well as turbine and wind tunnel geometry, are published in detail and institutions, which develop or work with CFD simulations are invited to predict the test cases without knowing the results. The blindly submitted numerical predictions are compared to the experimental results to analyze the accuracy of the simulations and to identify sources for deviations among the different techniques.

The first Blind test focused on a single turbine and modelers were asked to predict its performance as well as the mean streamwise velocity and turbulent kinetic energy in the wake for distances from $1D$ to $5D$ behind the turbine. The Blind test attracted eight different research groups who submitted simulations of various types ranging from Reynolds-Averaged-Navier-Stokes (RANS) simulations to Large-eddy simulations. The simulation results deviated significantly from the experimental results as reported by Krogstad and Eriksen (2013). Whereas the spread in performance around the experimental results were considerable, the predictions of wake turbulence were scattered by several orders of magnitude. In the next Blind test a second turbine, operating in the wake of the first turbine, was added to increase the test complexity. The participants were asked to simulate the performance of both turbines with the focus on the downstream turbine operating in the wake. Furthermore, the modelers were asked to simulate the wake formed behind the downstream turbine. For this Blind test nine predictions were submitted. The results reported by Pierella et al. (2014) show a large spread in the performance of the downstream turbine and the predictions of the wake properties varied significantly for the different simulations. In the third Blind test the complexity was again increased by applying a lateral offset of half a rotor diameter to the same turbine array as in Blind test 2. The results reported in Krogstad et al. (2015) show an improvement in the performance predictions, which contained only a small scatter around the experimental result. However, the simulations of the asymmetric wake still contained large uncertainties in predicting turbulence. The fourth Blind test focused on the influence of different inflow conditions. Therefore, the wake behind a single turbine was investigated up to $9D$ behind the upstream turbine for low-turbulent, high-turbulent and turbulent shear inflow. Furthermore, the performance of an aligned turbine array was investigated. The five research groups,

which submitted numerical results for this Blind test, managed to predict the performance of the upstream turbine fairly well. However, the more complicated predictions of the downstream turbine's performance still contained a significant scatter. The results presented by Bartl and Sætran (2017) show that the mean wake properties were generally predicted well. Nevertheless, the turbulence predictions still showed a large discrepancy between experimental and numerical results.

In the fifth Blind test, which is presented in *Paper VII* the performance and the wake flow of two different single yawed turbines and a turbine array with a yawed upstream turbine were compared in three test cases. In the first test case the modelers were asked to predict power, thrust and yaw moments of the yawed NTNU turbine LARS1 and the wake flow at $3D$ and $6D$ behind the turbine. For the second test case the non-yawed NTNU turbine T2 was placed $3D$ behind the yawed turbine and the power, thrust and yaw moments of the downstream turbine as well as the wake flow $3D$ behind the turbine were investigated. The third test case was similar to the first test case. Only the NTNU turbine was replaced by the ForWind turbine, which has a somewhat smaller rotor diameter and a different rotor design. The modelers were asked to provide predictions for the streamwise and vertical velocity component as well as the turbulent kinetic energy, at the defined downstream distances in full wake planes. The numerical and experimental results were compared visually and also by applying different statistical methods to get quantitative information about the deviations.

The Blind test attracted four institutions who submitted results for the three test cases. The predictions for the power, thrust and yaw moments show significant deviations from the experimental results. The scatter was larger than observed in previous Blind tests, suggesting that the simulations had problems with the increased complexity of unsteady blade loading due to the yawed turbine operation. The comparison of the wake flow generally showed very good agreement between the experimental data and the numerical predictions. The general features such as the wake shape and deflection were predicted well by all the simulations. Also the streamwise velocity in the wake was predicted fairly accurate by all simulations. Even though it is difficult to predict the flow in vertical direction because of its low magnitude, the complex patterns of the vertical velocity component were accurately predicted by all simulations in general. The same applies for the turbulent kinetic energy in the wake behind the single turbine and the two-turbine array. Whereas previous Blind tests showed that it is difficult to predict the wake turbulence, all simulations managed to predict the turbulent kinetic energy accurately.

The results of this Blind test comparison confirmed the continuous improvement in performance and wake flow predictions from Blind test 1 to Blind test 5. Furthermore, they showed that the different simulation techniques were able to perform accurate

predictions, also for complex setups featuring highly unsteady flow in yawed and partial wake operation.

Chapter 4

Conclusions

The present PhD thesis investigated rotor-wake interactions and analyzed the potential of different concepts for the optimization of wind farms. For this purpose, performance and loads of model wind turbines as well as their wake characteristics were measured in a number of experimental wind tunnel studies. In the scope of the thesis, the wake flows behind rotors of different number of blades, different rotational direction and additional winglets on the wing tips were investigated to investigate how the different rotor designs could affect the wake characteristics and effects on turbines operated in the wake. In the second part of the thesis, the wake behind a yawed turbine was investigated for different inflow conditions and yaw angles. The potential of intentional yaw misalignment for wind farm control optimization was thereafter analyzed for a setup of two aligned and laterally offset turbines. The wake flow data was furthermore used as reference data in a blind test experiment, to which numerical predictions were compared and deficits in the CFD codes identified. The comparison of wakes behind a 2- and 3-bladed rotor of the same thrust loading showed a minor difference in the mean streamwise velocity development. The peak levels of rotor-generated turbulence were, however, observed to be lower for a three-bladed rotor in the near wake. In general, it could be concluded, that the blade number of similar rotor designs did not noticeably affect the wake flow and thus would not have any significantly influence the overall wind farm power.

An investigation of a counter-rotating array of two turbines showed only a small potential for power optimization. A slightly improved combined performance was attributed to higher angles of attack on the counter-rotating downstream turbine. Therefore, similar performance increases could be potentially obtained by downstream turbine pitch control.

An attachment of optimized winglets on the blade tips of a two-bladed rotor could raise the power coefficient C_P by 8.9%, while the thrust coefficient C_T was observed to increase only moderately by 7.4% at the same time. Moreover, an analysis of the wake behind a wingletted rotor showed a significant influence on the tip region, while the energy content in the wake was almost identical for the two rotor concepts. The total kinetic energy was found to be initially higher in the tip region, when winglets were attached to the rotor tips. An analysis of the phase-averaged vorticity in the tip region disclosed an earlier interaction of the tip vortices behind the wingletted rotor. The vortex pairing caused an earlier expansion of the shear layer in the tip region, leading to a slightly faster wake recovery.

The second part of this thesis, confirmed that intentional yaw misalignment of a turbine laterally deflects the wake downstream of the rotor due to a lateral component of the thrust vector. Furthermore, it was shown that the level of inflow turbulence affected the curled shape and also the overall deflection of the wake. Moreover, the wake shape was found to be significantly asymmetric for positive and negative yaw angles of the upstream rotor. By steering the wake away from a downstream turbine the performance of a turbine array could be increased by up to 11%. However, the yaw moments acting on the yawed turbine and the downstream turbine operating in a partial wake were observed to increase, which emphasized the importance of also considering loads when applying yaw control for the power optimization of wind farms. A possibility to reduce loads with yaw control was demonstrated to be an opposite yawing of the downstream turbine operated in a partial wake. This strategy was found to decrease loads on the downstream turbine while the total power output was slightly increased. In conclusion, the study showed a large potential of intentional yaw misalignment for optimizing wind farm control.

A comparison of numerical predictions to experimental reference data in the Blind test confirmed the ability of Large-Eddy based CFD codes to predict mean velocities and turbulent kinetic energy levels in the wake accurately.

Future work

As highlighted above, yaw control was seen to be a very promising method for the power optimization of wind farms. For this reason, it is recommended that further research should focus on this topic. As accurate numerical predictions were obtained in the Blind test experiment, further quantities could be extracted from these simulations. An investigation of the detailed rotor loads acting on a turbine in different yaw configurations is recommended. Furthermore, the loads acting on a downstream

turbine operated in a partial wake are deemed to be crucial to be assessed for a holistic optimization of a yaw-controlled wind farm.

Furthermore, the effects of winglets on the individual blade loads could be investigated in more detail. It is expected that the loads in the blade tip region rise and consequently increase the blade root bending moments. This is of importance for an optimization process of a rotor, in which a trade-off between power gains and increased structural loads must be achieved.

References

Verogray RGD850, Stratasys, safety data sheet, revision A, 2nd March 2016, 2016.

Adaramola, M. and Krogstad, P.-Å.: Experimental investigation of wake effects on wind turbine performance, Renewable Energy, 36, 2078–2086, doi:10.1016/j.renene.2011.01.024, 2011.

Ainslie, J.: Calculating the flowfield in the wake of wind turbines, Journal of Wind Engineering and Industrial Aerodynamics, 27, 213 – 224, doi:doi.org/10.1016/0167-6105(88)90037-2, 1988.

Ammara, I., Leclerc, C., and Masson, C.: A viscous three-dimensional differential/actuator-disk method for the aerodynamic analysis of wind farms, Journal of Solar Energy Engineering, 124, 345–356, doi:10.1115/1.1510870, 2002.

Barthelmie, R. J., Larsen, G. C., Frandsen, S. T., Folkerts, L., Rados, K., Pryor, S. C., Lange, B., and Schepers, G.: Comparison of Wake Model Simulations with Offshore Wind Turbine Wake Profiles Measured by Sodar, Journal of Atmospheric and Oceanic Technology, 23, 888–901, doi:10.1175/JTECH1886.1, 2006.

Barthelmie, R. J., Frandsen, S. T., Nielsen, M. N., Pryor, S. C., Rethore, P.-E., and Jørgensen, H. E.: Modelling and measurements of power losses and turbulence intensity in wind turbine wakes at Middelgrunden offshore wind farm, Wind Energy, 10, 517–528, doi:10.1002/we.238, 2007.

Barthelmie, R. J., Hansen, K., Frandsen, S. T., Rathmann, O., Schepers, J. G., Schlez, W., Phillips, J., Rados, K., Zervos, a., Politis, E. S., and Chaviaropoulos, P. K.: Modelling and measuring flow and wind turbine wakes in large wind farms offshore, Wind Energy, 12, 431–444, doi:10.1002/we.348, 2009.

Bartl, J. and Sætran, L.: Blind test comparison of the performance and wake flow between two in-line wind turbines exposed to different turbulent inflow conditions, Wind Energy Science, 2, 55–76, doi:10.5194/wes-2-55-2017, 2017.

Bartl, J. and Sætran, L.: Experimental testing of axial induction based control strategies for wake control and wind farm optimization, Journal of Physics: Conference Series, 753, 032 035, doi:10.1088/1742-6596/753/3/032035, 2016.

Bartl, J., Pierella, F., and Sætrana, L.: Wake Measurements Behind an Array of Two Model Wind Turbines, Energy Procedia, 24, 305 – 312, doi:10.1016/j.egypro.2012.06.113, 2012.

Bastankhah, M. and Porté-Agel, F.: Experimental and theoretical study of wind turbine wakes in yawed conditions, Journal of Fluid Mechanics, 806, 506–541, doi:10.1017/jfm.2016.595, 2016.

Benedict, L. H. and Gould, R. D.: Towards better uncertainty estimates for turbulence statistics, Experiments in Fluids, 22, 129–136, doi:10.1007/s003480050030, 1996.

Betz, A.: Wind-Energie und ihre Ausnutzung durch Windmühlen, Vandenhoeck, 1926.

Chamorro, L. P. and Porté-Agel, F.: A Wind-Tunnel Investigation of Wind-Turbine Wakes: Boundary-Layer Turbulence Effects, Boundary-Layer Meteorology, 132, 129–149, doi:10.1007/s10546-009-9380-8, 2009.

Chen, T. and Liou, L.: Blockage corrections in wind tunnel tests of small horizontal-axis wind turbines, Experimental Thermal and Fluid Science, 35, 565 – 569, doi:10.1016/j.expthermflusci.2010.12.005, 2011.

Corten, G., Schaak, P., and Hegberg, T.: Turbine Interaction in Large Offshore Wind Farms; Wind Tunnel Measurements, ECN Wind Energy, ECN-C–04-048, 2004.

Crespo, A., Hernández, J., and Frandsen, S.: Survey of modelling methods for wind turbine wakes and wind farms, Wind Energy, 2, 1–24, doi:10.1002/(SICI)1099-1824(199901/03)2:1<1::AID-WE16>3.0.CO;2-7, 1999.

Drela, M.: XFOIL: An Analysis and Design System for Low Reynolds Number Airfoils. Low Reynolds Number Aerodynamics, Springer-Verlag, lecture notes in Eng. 54., 1989.

Eriksen, P. E. and Krogstad, P.: An experimental study of the wake of a model wind turbine using phase-averaging, International Journal of Heat and Fluid Flow, 67, 52 – 62, doi:10.1016/j.ijheatfluidflow.2017.05.002, 2017a.

Eriksen, P. E. and Krogstad, P.-Å.: Development of coherent motion in the wake of a model wind turbine, Renewable Energy, 108, 449 – 460, doi:10.1016/j.renene.2017.02.031, 2017b.

Fleming, P., Gebraad, P. M., Lee, S., van Wingerden, J.-W., Johnson, K., Churchfield, M., Michalakes, J., Spalart, P., and Moriarty, P.: Simulation comparison of wake mitigation control strategies for a two-turbine case, Wind Energy, 18, 2135–2143, doi:10.1002/we.1810, 2015.

Fleming, P., Churchfield, M., Scholbrock, A., Clifton, A., Schreck, S., Johnson, K., Wright, A., Gebraad, P., Annoni, J., Naughton, B., Berg, J., Herges, T., White, J., Mikkelsen, T., Sjöholm, M., and Angelou, N.: Detailed field test of yaw-based wake steering, Journal of Physics: Conference Series, 753, 052 003, doi:10.1088/1742-6596/753/5/052003, 2016a.

Fleming, P. a., Gebraad, P. M. O., Lee, S., van Wingerden, J. W., Johnson, K., Churchfield, M., Michalakes, J., Spalart, P., and Moriarty, P.: Evaluating techniques for redirecting turbine wakes using SOWFA, Renewable Energy, 70, 211–218, doi:10.1016/j.renene.2014.02.015, 2014.

Fleming, P. A., Ning, A., Gebraad, P. M. O., and Dykes, K.: Wind plant system engineering through optimization of layout and yaw control, Wind Energy, 19, 329–344, doi:10.1002/we.1836, 2016b.

Freitag, W. and Schulze, E. T.: Blended Winglets Improve Performance, AERO-MAGAZINE, 35, 2009.

Gaunaa, M. and Johansen, J.: Determination of the Maximum Aerodynamic Efficiency of Wind Turbine Rotors with Winglets, Journal of Physics: Conference Series, 75, 012 006, doi:10.1088/1742-6596/75/1/012006, 2007.

Gebraad, P. M. O., Teeuwisse, F. W., van Wingerden, J. W., Fleming, P. A., Ruben, S. D., Marden, J. R., and Pao, L. Y.: Wind plant power optimization through yaw control using a parametric model for wake effects—a CFD simulation study, Wind Energy, 19, 95–114, doi:10.1002/we.1822, 2014.

Gebraad, P. M. O., Teeuwisse, F. W., van Wingerden, J. W., Fleming, P. A., Ruben, S. D., Marden, J. R., and Pao, L. Y.: Wind plant power optimization through yaw control using a parametric model for wake effects—a CFD simulation study, Wind Energy, 19, 95–114, doi:10.1002/we.1822, 2016.

Gertz, D., Johnson, D. A., and Swytink-Binnema, N.: An Evaluation Testbed for Wind Turbine Blade Tip Designs—Winglet Results, Wind Engineering, 36, 389–410, 2012.

Gertz, D., Johnson, D. A., and Swytink-Binnema, N.: Comparative Measurements of the Effect of a Winglet on a Wind Turbine, in: Wind Energy - Impact of Turbulence, edited by Hölling, M., Peinke, J., and Ivanell, S., pp. 121–126, Springer Berlin Heidelberg, Berlin, Heidelberg, 2014.

GWEC: Global Wind Report 2016-Annual Market Update. 2016, 2017.

Hansen, K. S., Barthelmie, R. J., Jensen, L. E., and Sommer, A.: The impact of turbulence intensity and atmospheric stability on power deficits due to wind turbine wakes at Horns Rev wind farm, Wind Energy, 15, 183–196, doi:10.1002/we.512, 2012.

Hansen, M. O.: Aerodynamics of wind turbines, Routledge, 2015.

Hau, E.: Wind turbines: fundamentals, technologies, application, economics, Springer-Verlag Berlin Heidelberg, 3 edn., doi:10.1007/978-3-642-27151-9, 2013.

Højstrup, J.: Spectral coherence in wind turbine wakes, Journal of Wind Engineering and Industrial Aerodynamics, 80, 137 – 146, doi:https://doi.org/10.1016/S0167-6105(98)00198-6, 1999.

Hooper, J. and Musgrove, A.: Reynolds stress, mean velocity, and dynamic static pressure measurement by a four-hole pressure probe, Experimental Thermal and Fluid Science, 15, 375 – 383, doi:10.1016/S0894-1777(97)00005-8, 1997.

Howland, M. F., Bossuyt, J., Martínez-Tossas, L. A., Meyers, J., and Meneveau, C.: Wake structure in actuator disk models of wind turbines in yaw under uniform inflow conditions, Journal of Renewable and Sustainable Energy, 8, 043 301, doi:10.1063/1.4955091, 2016.

IEA: Energy, climate change and environment 2016 insights, IEA Publications, Paris,France, 2016.

IEA: World Energy Outlook 2017, Organisation for Economic Co-operation and Development, OECD, 2017.

IPCC: Climate change 2014: mitigation of climate change. Contribution of Working Group III to the Fifth Assessment Report of the Intergovernmental Panel on Climate Change [Edenhofer, O., R. Pichs-Madruga, Y. Sokona, E. Farahani, S. Kadner, K. Seyboth, A. Adler, I. Baum, S. Brunner, P. Eickemeier, B. Kriemann, J. Savolainen, S. Schlömer, C. von Stechow, T. Zwickel and J.C. Minx (eds.)]., Cambridge University Press, Cambridge, United Kingdom and New York, NY, USA, 2014.

Jiménez, n., Crespo, A., and Migoya, E.: Application of a LES technique to characterize the wake deflection of a wind turbine in yaw, Wind Energy, 13, 559–572, doi: 10.1002/we.380, 2010.

Johansen, J. and Sørensen, N. N.: Aerodynamic investigation of winglets on wind turbine blades using CFD, Denmark. Forskningscenter Risoe. Risoe-R, no. 1543(EN), iSSN 0106-2840, 2006.

Johansen, J. and Sørensen, N. N.: Numerical analysis of winglets on wind turbine blades using CFD, in: European Wind Energy Congress, Citeseer, 2007.

Knudsen, T., Bak, T., and Svenstrup, M.: Survey of wind farm control—power and fatigue optimization, Wind Energy, 18, 1333–1351, doi:10.1002/we.1760, 2014.

Krogstad, P.-Å. and Adaramola, M. S.: Performance and near wake measurements of a model horizontal axis wind turbine, Wind Energy, 15, 743–756, doi:10.1002/we.502, 2012.

Krogstad, P.-Å. and Eriksen, P. E.: "Blind test" calculations of the performance and wake development for a model wind turbine, Renewable Energy, 50, 325 – 333, doi:10.1016/j.renene.2012.06.044, 2013.

Krogstad, P. Å. and Lund, J.: An experimental and numerical study of the performance of a model turbine, Wind Energy, 15, 443–457, doi:10.1002/we.482, 2012.

Krogstad, P.-Å., Sætran, L., and Adaramola, M. S.: "Blind Test 3" calculations of the performance and wake development behind two in-line and offset model wind turbines, Journal of Fluids and Structures, 52, 65–80, doi:10.1016/j.jfluidstructs.2014.10.002, 2015.

Kumer, V.-M., Reuder, J., Svardal, B., Sætre, C., and Eecen, P.: Characterisation of Single Wind Turbine Wakes with Static and Scanning WINTWEX-W LiDAR Data, Energy Procedia, 80, 245 – 254, doi:10.1016/j.egypro.2015.11.428, 2015.

Maniaci, D. and Maughmer, M.: Winglet design for wind turbines using a free-wake vortex analysis method, in: 50th AIAA Aerospace Sciences Meeting including the New Horizons Forum and Aerospace Exposition, p. 1158, doi:10.2514/6.2012-1158, 2012.

Manwell, J. F., McGowan, J. G., and Rogers, A. L.: Wind energy explained: theory, design and application, John Wiley & Sons, 2 edn., 2010.

Medici, D. and Alfredsson, P. H.: Measurements on a wind turbine wake: 3D effects and bluff body vortex shedding, Wind Energy, 9, 219–236, doi:10.1002/we.156, 2006.

Miller, M., Kiefer, J., Westergaard, C., and Hultmark, M.: Model Wind Turbines Tested at Full-Scale Similarity, Journal of Physics: Conference Series, 753, 032 018, doi:10.1088/1742-6596/753/3/032018, 2016.

Mosetti, G., Poloni, C., and Diviacco, B.: Optimization of wind turbine positioning in large windfarms by means of a genetic algorithm, Journal of Wind Engineering and Industrial Aerodynamics, 51, 105 – 116, doi:https://doi.org/10.1016/0167-6105(94)90080-9, 1994.

Newman, A. J., Cal, R. B., and Castillo, L.: Blade number effects in a scaled down wind farm, Renewable Energy, 81, 472 – 481, doi:10.1016/j.renene.2015.03.013, 2015.

Ostovan, Y.: Winglets for wind turbines: An experimental study on aerodynamic performance and tip vortex behavior, Ph.D. thesis, Middle East Technical University, 2017.

Pierella, F. and Sætran, L.: Wind tunnel investigation on the effect of the turbine tower on wind turbines wake symmetry, Wind Energy, 20, 1753–1769, doi:10.1002/we.2120, 2017.

Pierella, F., Krogstad, P.-Å., and Sætran, L.: Blind Test 2 calculations for two in-line model wind turbines where the downstream turbine operates at various rotational speeds, Renewable Energy, 70, 62 – 77, doi:10.1016/j.renene.2014.03.034, special issue on aerodynamics of offshore wind energy systems and wakes, 2014.

Polster, F., Bartl, J., Mühle, F., Thamsen, P. U., and Sætran, L.: Experimental validation of analytical wake and downstream turbine performance modelling, Journal of Physics: Conference Series, manuscript submitted for publication, 2017.

Quinn, R., Schepers, G., and Bulder, B.: A Parametric Investigation Into the Effect of Low Induction Rotor (LIR) Wind Turbines on the Levelised Cost of Electricity for a 1 GW Offshore Wind Farm in a North Sea Wind Climate, Energy Procedia, 94, 164 – 172, doi:10.1016/j.egypro.2016.09.213, 2016.

Raach, S., Schlipf, D., Borisade, F., and Cheng, P. W.: Wake redirecting using feedback control to improve the power output of wind farms, in: 2016 American Control Conference (ACC), pp. 1387–1392, doi:10.1109/ACC.2016.7525111, 2016.

Raach, S., Schlipf, D., and Cheng, P. W.: Lidar-based wake tracking for closed-loop wind farm control, Wind Energy Science, 2, 257–267, doi:10.5194/wes-2-257-2017, 2017.

Reuder, J., Båserud, L., Kral, S., Kumer, V., Wagenaar, J. W., and Knauer, A.: Proof of Concept for Wind Turbine Wake Investigations with the RPAS SUMO, Energy Procedia, 94, 452 – 461, doi:10.1016/j.egypro.2016.09.215, 2016.

Ryi, J., Rhee, W., Hwang, U. C., and Choi, J.-S.: Blockage effect correction for a scaled wind turbine rotor by using wind tunnel test data, Renewable Energy, 79, 227 – 235, doi:10.1016/j.renene.2014.11.057, selected Papers on Renewable Energy: AFORE 2013, 2015.

S. Lissaman, P.: Energy effectiveness of arbitrary arrays of wind turbines, Journal of Energy, 3, 323–328, doi:10.2514/3.62441, 1979.

Sanderse, B.: Aerodynamics of Wind Turbine Wakes: Literature Review, vol. ECN-E–09-016 of *ECN.: E-series*, ECN Wind Energy, 2009.

Sanderse, B., van der Pijl, S., and Koren, B.: Review of computational fluid dynamics for wind turbine wake aerodynamics, Wind Energy, 14, 799–819, doi:10.1002/we.458, 2011.

Sarlak, H., Nishino, T., Martínez-Tossas, L., Meneveau, C., and Sørensen, J.: Assessment of blockage effects on the wake characteristics and power of wind turbines, Renewable Energy, 93, 340 – 352, doi:10.1016/j.renene.2016.01.101, 2016.

Schottler, J., Hölling, A., Peinke, J., and Hölling, M.: Design and implementation of a controllable model wind turbine for experimental studies, Journal of Physics: Conference Series, 753, 072 030, doi:10.1088/1742-6596/753/7/072030, 2016a.

Schottler, J., Hölling, A., Peinke, J., and Hölling, M.: Wind tunnel tests on controllable model wind turbines in yaw, AIAA 34th Wind Energy Symposium, doi:10.2514/6.2016-1523, 2016b.

Schottler, J., Hölling, A., Peinke, J., and Hölling, M.: Brief communication: On the influence of vertical wind shear on the combined power output of two model wind turbines in yaw, Wind Energy Science, 2, 439–442, doi:10.5194/wes-2-439-2017, 2017.

Schottler, J., Bartl, J., and Mühle, F.: Wind tunnel experiments on wind turbine wakes in yaw, doi:10.5281/zenodo.1193656, 2018.

Schreiber, J., Nanos, E. M., Campagnolo, F., and Bottasso, C. L.: Verification and Calibration of a Reduced Order Wind Farm Model by Wind Tunnel Experiments, Journal of Physics: Conference Series, 854, 012 041, doi:10.1088/1742-6596/854/1/012041, 2017.

Schümann, H., Pierella, F., and Sætran, L.: Experimental Investigation of Wind Turbine Wakes in the Wind Tunnel, Energy Procedia, 35, 285 – 296, doi:10.1016/j.egypro.2013.07.181, 2013.

Shakoor, R., Hassan, M. Y., Raheem, A., and Wu, Y.-K.: Wake effect modeling: A review of wind farm layout optimization using Jense's model, Renewable and Sustainable Energy Reviews, 58, 1048 – 1059, doi:https://doi.org/10.1016/j.rser.2015.12.229, 2016.

Shepherd, I. C.: A four hole pressure probe for fluid flow measurements in three dimensions, Journal of Fluids Engineering, 103, 590–594, doi:10.1115/1.3241774, 1981.

Somers, D. M.: The S825 and S826 airfoils, National Renewable Energy Laboratory, Subcontractor Report, last access 03.11.2017, 2005.

Steinbuch, M., de Boer, W., Bosgra, O., Peters, S., and Ploeg, J.: Optimal control of wind power plants, Journal of Wind Engineering and Industrial Aerodynamics, 27, 237 – 246, doi:https://doi.org/10.1016/0167-6105(88)90039-6, 1988.

Thomsen, K. and Sørensen, P.: Fatigue loads for wind turbines operating in wakes, Journal of Wind Engineering and Industrial Aerodynamics, 80, 121 – 136, doi:10.1016/S0167-6105(98)00194-9, 1999.

Tobin, N., Hamed, A. M., and Chamorro, L. P.: An Experimental Study on the Effects ofWinglets on the Wake and Performance of a ModelWind Turbine, Energies, 8, 11 955–11 972, doi:doi:10.3390/en81011955, 2015.

Trujillo, J. J., Seifert, J. K., Würth, I., Schlipf, D., and Kühn, M.: Full-field assessment of wind turbine near-wake deviation in relation to yaw misalignment, Wind Energy Science, 1, 41–53, doi:10.5194/wes-1-41-2016, 2016.

UNFCCC: Adoption of the Paris Agreement. Proposal by the President, United Nations Office at Geneva, Geneva, Switzerland, 2015.

van Kuik, G. A. M., Peinke, J., Nijssen, R., Lekou, D., Mann, J., Sørensen, J. N., Ferreira, C., van Wingerden, J. W., Schlipf, D., Gebraad, P., Polinder, H., Abrahamsen, A., van Bussel, G. J. W., Sørensen, J. D., Tavner, P., Bottasso, C. L., Muskulus, M., Matha, D., Lindeboom, H. J., Degraer, S., Kramer, O., Lehnhoff, S., Sonnenschein,

M., Sørensen, P. E., Künneke, R. W., Morthorst, P. E., and Skytte, K.: Long-term research challenges in wind energy - a research agenda by the European Academy of Wind Energy, Wind Energy Science, 1, 1–39, doi:10.5194/wes-1-1-2016, 2016.

Vermeer, L. J., Sørensen, J. N., and Crespo, a.: Wind turbine wake aerodynamics, Progress in Aerospace Sciences, 39, 467–510, doi:10.1016/S0376-0421(03)00078-2, 2003.

Vollmer, L., Steinfeld, G., Heinemann, D., and Kühn, M.: Estimating the wake deflection downstream of a wind turbine in different atmospheric stabilities: an LES study, Wind Energy Science, 1, 129–141, doi:10.5194/wes-1-129-2016, 2016.

Wang, J., Foley, S., Nanos, E. M., Yu, T., Campagnolo, F., Bottasso, C. L., Zanotti, A., and Croce, A.: Numerical and experimental study of wake redirection techniques in a boundary layer wind tunnel, Journal of Physics: Conference Series, 854, 012 048, doi:10.1088/1742-6596/854/1/012048, 2017.

Wharton, S. and Lundquist, J. K.: Assessing atmospheric stability and its impacts on rotor-disk wind characteristics at an onshore wind farm, Wind Energy, 15, 525–546, doi:10.1002/we.483, 2012.

Wheeler, A. and Ganji, A.: Introduction to Engineering Experimentation, Pearson Education, Upper Saddle River, New Jersey, USA, third edition edn., 2010.

Windpowermonthly: Ten of the biggest turbines, URL https://www.windpowermonthly.com/10-biggest-turbines, accessed: 2018-02-09, 2017.

Yuan, W., Ozbay, A., Tian, W., and Hu, H.: An experimental investigation on the effects of turbine rotation directions on the wake interference of wind turbines, in: 51st AIAA Aerospace Sciences Meeting including the New Horizons Forum and Aerospace Exposition, p. 607, doi:10.2514/6.2013-607, 2013.

Yuan, W., Tian, W., Ozbay, A., and Hu, H.: An experimental study on the effects of relative rotation direction on the wake interferences among tandem wind turbines, Science China Physics, Mechanics & Astronomy, 57, 935–949, doi:10.1007/s11433-014-5429-x, 2014.

Appendix A

Technical drawings

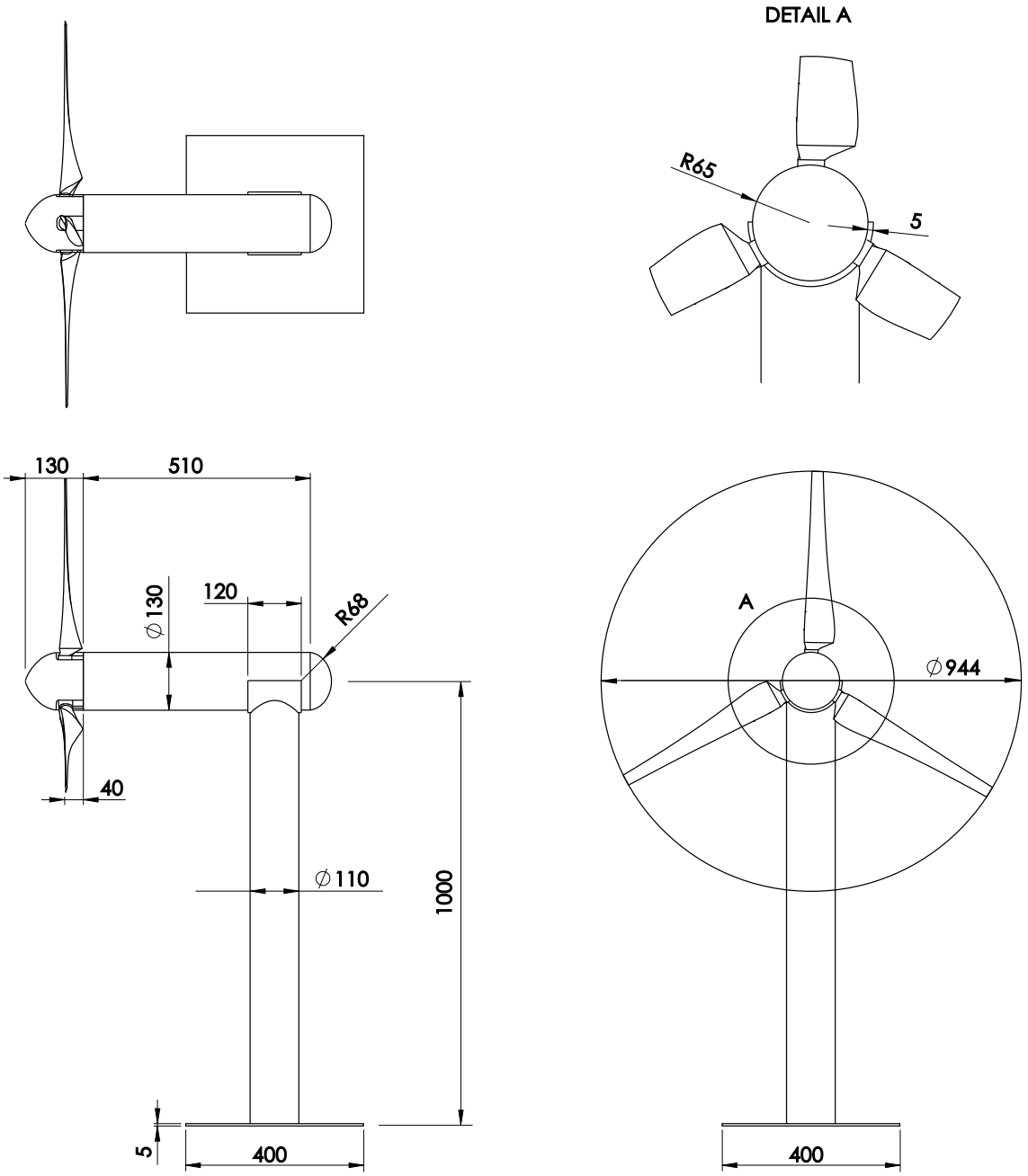

Figure A.1: Technical drawing of NTNU model wind turbine T1.

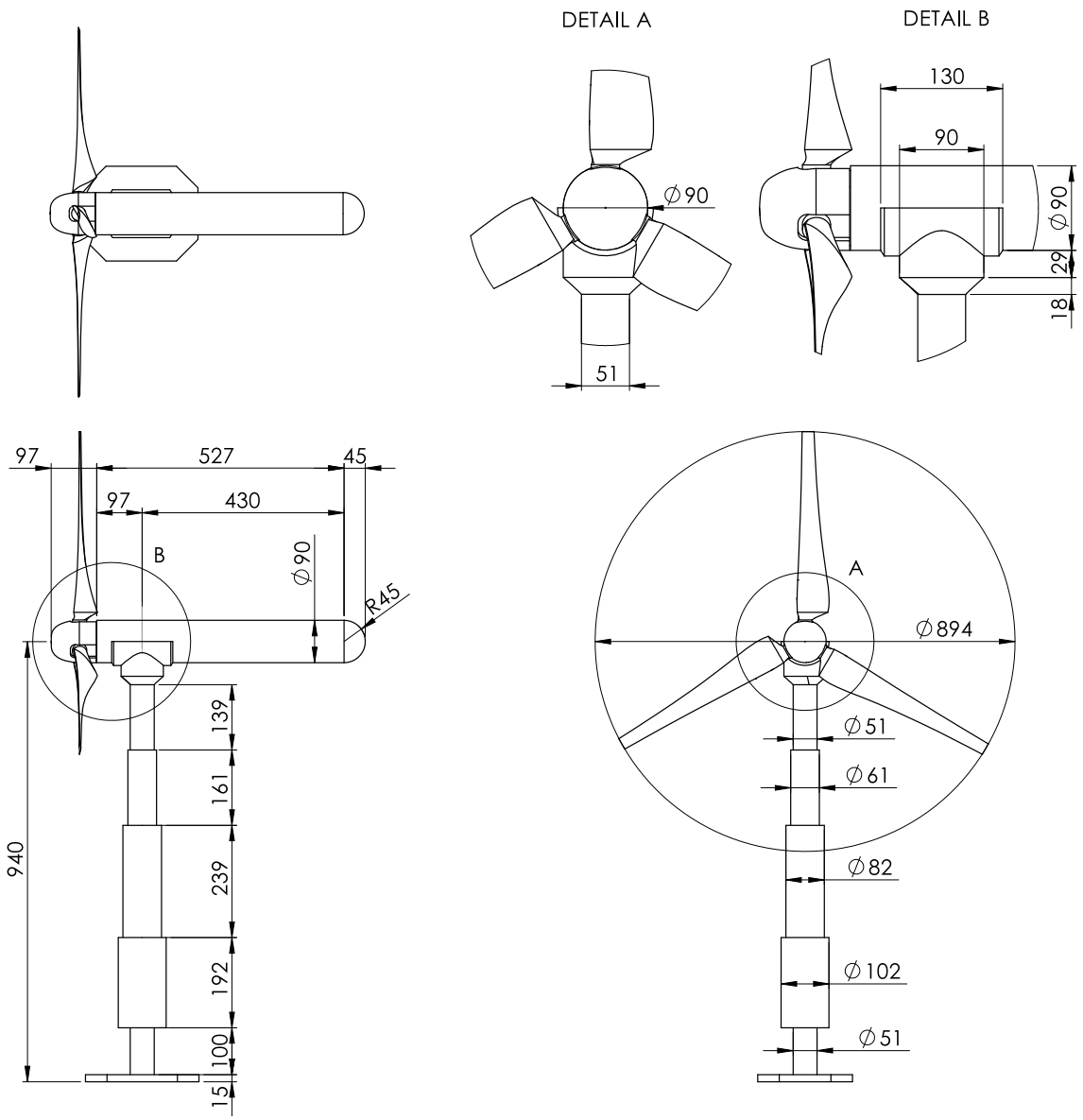

Figure A.2: Technical drawing of NTNU model wind turbine T2.

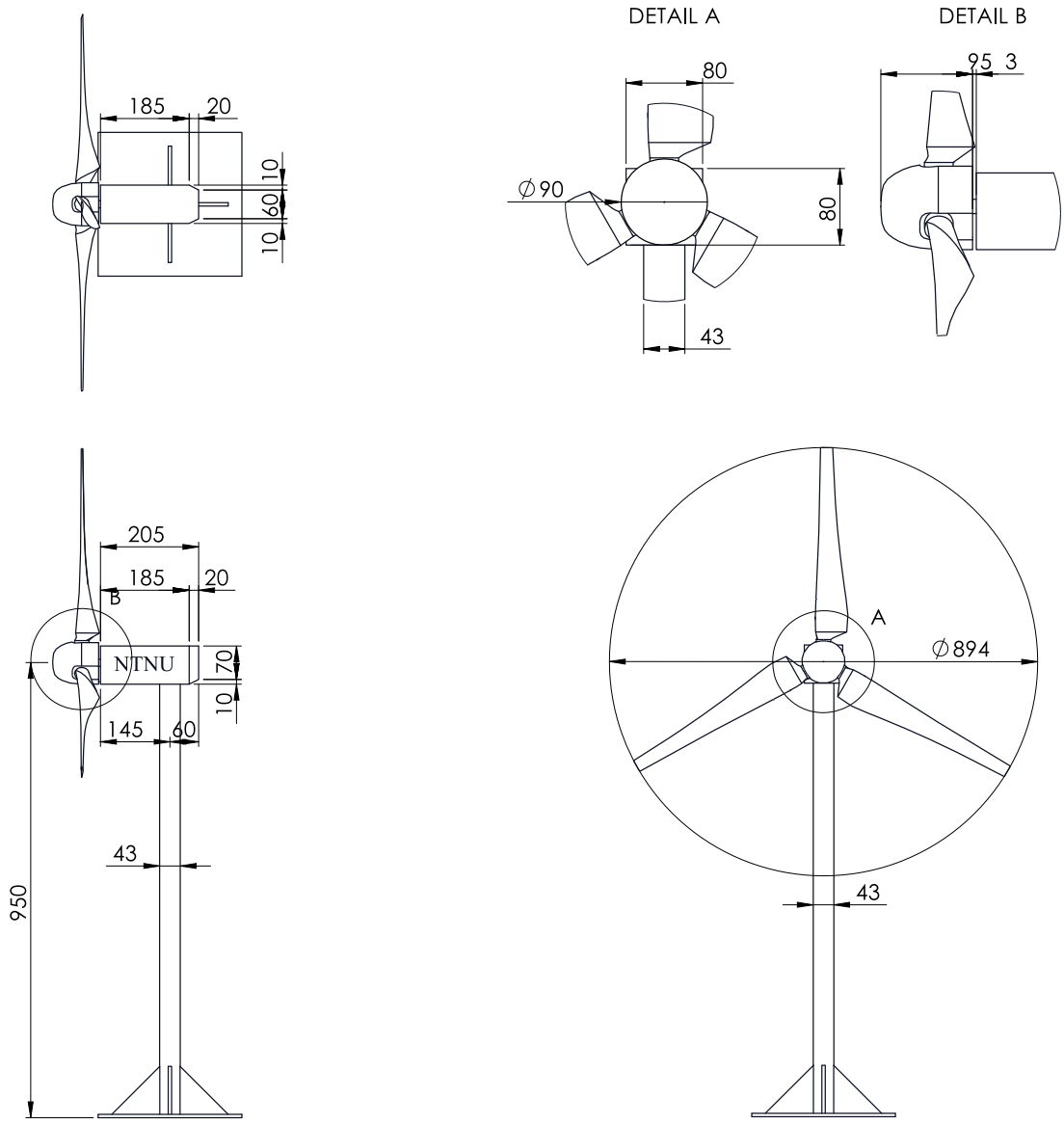

Figure A.3: Technical drawing of NTNU model wind turbine LARS1.

Paper I
Mühle, F., Adaramola, M.S. & Sætran, L. 2016. The effect of the number of blades on wind turbine wake – a comparison between 2-and 3-bladed rotors. - Journal of Physics: Conference Series 753: 032017, 10 pp.
DOI: 10.1088/1742-6596/753/3/032017

Paper II
Mühle, F., Adaramola, M.S. & Sætran, L. 2017. The effect of rotational direction on the wake of a wind turbine rotor – a comparison study of aligned co- and counter rotating turbine arrays. - Energy Procedia 137: 238–245.
DOI: 10.1016/j.egypro.2017.10.346

Paper III
Mühle, F., Bartl, J., Hansen, T., Adaramola, M.S. & Sætran, L. An experimental study on the effect of winglets on the tip vortex interaction in the near wake of a model wind turbine.
(Manuscript)

Paper IV
Hansen, T.H. & Mühle, F. 2018. Winglet optimization for a model-scale wind turbine. - Wind Energy 21: 634-649.
DOI: 10.1002/we.2183

Paper V
Bartl, J., Mühle, F., Schottler, J., Sætran, L., Peinke, J., Adaramola, M.S. & Hölling, M. 2018. Wind tunnel experiments on wind turbine wakes in yaw: effects of inflow turbulence and shear. - Wind Energy Science 3: 329-343.
DOI: 10.5194/wes-3-329-2018

Paper VI
Bartl, J., Mühle, F. & Sætran, L. 2018. Wind tunnel study on power output and yaw moments for two yaw-controlled model wind turbines. - Wind Energy Science 3: 489-502.
DOI: 10.5194/wes-3-489-2018

Paper VII
Mühle, F., Schottler, J., Bartl, J., Futrzynski, R., Evans, S., Bernini, L., Schito, P., Draper, M., Guggeri, A., Kleusberg, E., Henningson, D.S., Hölling, M., Peinke, J., Adaramola, M.S. & Sætran, L. Blind test comparison on the wake behind a yawed wind turbine. - Wind Energy Science.
(Under review), DOI: 10.5194/wes-2018-30

ISBN: 978-82-575-1762-5
ISSN: 1894-6402

Norwegian University
of Life Sciences

Postboks 5003
NO-1432 Ås, Norway
+47 67 23 00 00
www.nmbu.no

99564 / ANDVORDGRAFISK.NO